Ocean Modelling 27 (2009) 54–69

Contents lists available at ScienceDirect

Ocean Modelling

journal homepage: www.elsevier.com/locate/ocemod

Simulating the mass balance and salinity of Arctic and Antarctic sea ice. 2. Importance of sea ice salinity variations

Martin Vancoppenolle *, Thierry Fichefet, Hugues Goosse

Institut d'Astronomie et de Géophysique G. Lemaître, Université catholique de Louvain, Louvain-la-Neuve, Belgium

ARTICLE INFO

Article history:
Received 27 February 2008
Received in revised form 20 October 2008
Accepted 3 November 2008
Available online 21 November 2008

Keywords:
Sea ice
Model
Thickness
Salinity
Age
Arctic
Antarctic

ABSTRACT

Sea ice has a non-zero salinity that varies in space and time. This affects the sea ice thermal properties as well as the ice–ocean salt and freshwater exchanges, which may influence the sea ice mass balance and the polar oceans' characteristics. However, current sea ice models neglect or misrepresent the ice salinity. In this paper, we address the question of the importance of large-scale sea ice salinity variations for the sea ice mass balance and the upper ocean. To examine this question, we formulate salinity variations in the framework of the sea ice thickness distribution theory, using a simple parameterization for brine entrapment and drainage. The latter is tested one-dimensionally and then included in a three-dimensional large-scale ice–ocean model, OPA9-LIM3, which is run over 1970–2006, forced by a combination of atmospheric reanalyses and climatologies. Due to differences in the physical forcings, the model simulates Arctic and Antarctic sea ice salinity fields that profoundly differ, with a seasonal cycle that is found in reasonable agreement with available ice core data. Then, the role of salinity variations is analyzed by comparing the results of the simulation including the interactive salinity with several sensitivity runs using simpler representations of ice salinity. The simulated large-scale sea ice mass balance and upper ocean characteristics are found to be quite sensitive to the representation of ice salinity. In the Arctic, salinity variations induce changes in ice thickness up to one meter in some regions, due to modifications in the sea ice thermal properties. Around Antarctica, including salinity variations increases the simulated winter sea ice volume by up to 28% because of changes in ice–ocean interactions that stabilize the ocean. The model sensitivity to the sea ice salinity is of the same order of magnitude as a 10% change in bare ice albedo. Given the importance of salinity on the simulated sea ice characteristics, sea ice salinity variations should be included in assessments of the response of the high-latitude oceans to ongoing and future climate change.

1. Introduction

Sea ice is both an important actor in and an indicator of climate change (Serreze et al., 2007). It affects the radiative, heat and momentum exchanges between polar atmosphere and ocean (Holland et al., 2006a). Sea ice is also an habitat for marine organisms which lie at the basis of the polar foodweb (Thomas and Dieckmann, 2002) and modulates the atmosphere–ocean exchanges of CO_2 (e.g., Delille, 2006). Therefore, the role of sea ice in the carbon cycle is considered with increasing attention (e.g., Bates, 2006). In this context, the recent decrease in Arctic ice coverage (Cavalieri et al., 2003; Comiso, 2006) and thickness (Rothrock et al., 2008) – particularly over the summers of 2007 and 2008 – is striking. Climate projections for the next century (e.g., Arzel et al., 2006; Holland et al., 2006b) suggest that the decrease will continue in the future leading to a less extensive, thinner and younger Arctic sea ice cover. Those changes should in turn feedback on global climate and major biogeochemical cycles. In this framework, sea ice models, coupled to atmosphere and ocean general circulation models, are key tools to refine the present understanding of recent changes and projections of future state of sea ice.

Sea ice thickness is highly variable (0–20 m), even at subfloe scales, which is important, notably because the ice growth rate and the atmosphere–ocean heat exchanges non-linearly depend on ice thickness (Maykut, 1986). Large-scale sea ice models therefore assume a subgrid-scale ice thickness distribution (ITD) (see, e.g., Thorndike et al., 1975; Bitz et al., 2001). ITD physics combine numerous complex processes. Ice thermodynamics govern ice growth and melt (Maykut and Untersteiner, 1971) and induce smooth changes in the ITD. Mechanical processes induce sharper transitions in ITD, creating open water under diverging motion, and deforming the weakest thin ice by rafting or piling it into thick pressure ridges under converging motion. The summer ice-albedo

* Corresponding author.
E-mail address: vancop@astr.ucl.ac.be (M. Vancoppenolle).
URL: http://www.astr.ucl.ac.be/index.php?page=vancop%23HomePage (M. Vancoppenolle).

1463-5003/$ - see front matter © 2008 Elsevier Ltd. All rights reserved.
doi:10.1016/j.ocemod.2008.11.003

feedback critically depends on the melt of thin ice, which can only be represented through the use of an ITD. Hence, resolving the ITD greatly improves the climate simulations (Holland et al., 2006a).

Sea ice is a saline medium, for which salt, which cannot lock into the crystalline lattice, is dissolved into liquid inclusions of brine. Brine remains trapped in the ice during its formation and then drains back to the ocean as ice thickens and gets older (see, e.g., Cox and Weeks, 1988). Because of brine drainage, the sea ice salinity varies in time, vertically and horizontally.

Sea ice salinity is also characterized by large spatio-temporal variations. First, the sea ice salinity exhibits significant horizontal, subfloe-scale variations, driven by differences in ice thickness and snow cover and in the distribution of brine channels (Cottier et al., 1999; Eicken et al., 1991). Furthermore, due to the variable efficiency of brine entrapment and drainage, there are vertical variations in ice salinity (Malmgren, 1927; Schwarzacher, 1959; Nakawo and Sinha, 1981; Eicken, 1992; Jeffries and Porter, 1995). Finally, the ice salinity should logically present large-scale geographical variations, but to our knowledge, the latter have not yet been studied. The global ice cover salt content is determined by the combination of the salinity-thickness relation and the large-scale ITD.

Sea ice salinity may affect large-scale sea ice and ocean characteristics in two ways. First, in tight association with temperature, the ice salinity determines the brine-solid ice phase equilibrium (Frankenstein and Garner, 1967). Therefore, sea ice salinity variations induce large changes in the ice thermal properties (Notz, 2005; Pringle et al., 2007) that may affect the sea ice at a large scale (Vancoppenolle et al., 2006). In addition, salt and freshwater fluxes, respectively associated with ice growth and melt, strongly influence the oceanic density stratification and the World Ocean circulation (e.g., Aagaard and Carmack, 1989; Goosse and Fichefet, 1999). In spite of this potential importance, the sea ice models presently used for climate projections still neglect or misrepresent sea ice salinity variations (e.g., Fichefet and Morales Maqueda, 1997; Zhang and Rothrock, 2001; Bitz et al., 2001; Hunke and Lipscomb, 2004). Hence, the sensitivity of the large-scale sea ice features to ice salinity is unknown. The present paper addresses this issue.

Using a one-dimensional (1D) sea ice model in a climatological configuration and comparing the results of the simulation using an interactive halodynamic module (i.e., computing salinity variations) to simpler representations of sea ice salinity, Vancoppenolle et al. (2006) found differences in ice thickness up to 60 cm. In addition, they diagnosed significant differences in ice–ocean salt fluxes dominated by differences in growth and melt rates. However, as their model was 1D, excluded ITD, transport and oceanic feedbacks, no conclusion on the large-scale impact of sea ice salinity variations could be drawn.

The Vancoppenolle et al. (2006) study provides an incentive to test the role of salinity variations in a more complex model. In this paper, we introduce, validate and analyze the impact of a formulation of salinity variations in the 3D sea ice model LIM3.[1] In LIM3, the sea ice salinity affects ice thermodynamics and the ice–ocean salt and freshwater exchanges. In Section 2, we generalize the ITD theory to include ice salinity. Then, in Section 3, we validate the formulation of the thermodynamically driven changes in ice salinity produced by a simple parameterization and compare its results to the ones of a more complex, 1D, halodynamic sea ice model. Then, we include this parameterization in LIM3 (Section 4), validate the ice salinity simulated by LIM3 using this parameterization and analyze the resulting geographical ice salinity distribution (Section 5). Finally, in Section 6, we study the impact of salinity variations on the simulated sea ice and upper ocean characteristics.

2. Ice thickness and salinity distribution theory

First, it is necessary to extend the ITD theory to include the ice salinity. In order to account for unresolvable variations in ice thickness (h) in large-scale sea ice models, Thorndike et al. (1975) proposed to introduce an ITD function $g(h)$ defined by

$$\int_{h_1}^{h_2} g(h)dh = \frac{A(h_1,h_2)}{R}, \tag{1}$$

where R is the total area of the region of interest, $A(h_1, h_2)$ is the area in R covered by ice with thickness ranging between h_1 and h_2. Invoking continuity (i.e., assuming that $g(h)$ is valid for any subregion of R), Thorndike et al. argued that the conservation of ice mass can be written in the following way:

$$\frac{\partial g}{\partial t} = -\nabla \cdot (g\mathbf{u}) - \frac{\partial}{\partial h}(fg) + \psi^g, \tag{2}$$

where $\mathbf{u}$ is the two-dimensional horizontal ice velocity vector, f is the thermodynamic vertical growth rate (m/s) and ψ^g is the so-called mechanical redistribution function, which is a function of h and $g(h)$. ψ^g determines the changes in $g(h)$ during deformation events, redistributing ice area between the different thickness categories. The terms on the right-hand side of (2) respectively describe the effects on the ITD of (1) advection by the velocity field, (2) thermodynamic processes (growth and melt) and (3) mechanical processes (opening, rafting and ridging).

Any sea ice-related state variable has an associated distribution function which follows a conservation equation of the type (2), as suggested by Bitz et al. (2001) and Zhang and Rothrock (2001). Following similar arguments, we define the salinity distribution function s by

$$s(\lambda,\phi,h,t) = hg(\lambda,\phi,h,t)S(\lambda,\phi,h,t), \tag{3}$$

where S is the sea ice vertically-averaged ("bulk") salinity, λ is the longitude and ϕ the latitude. During transport and deformation, vertical variations in sea ice salinity are neglected. As g, s follows a conservation equation:

$$\frac{\partial s}{\partial t} = -\nabla \cdot (s\mathbf{u}) + \Theta^s + \psi^s. \tag{4}$$

The terms on the right-hand side of (4) respectively represent the effects of (1) horizontal advection, (2) halo-thermodynamics and (3) mechanical redistribution. The halo-thermodynamic term reads

$$\Theta^s = -\frac{\partial(fs)}{\partial h} + \theta^s. \tag{5}$$

The first term on the right-hand side is the transport in thickness space due to ice growth and melt, while the second one refers to brine entrapment and drainage. The latter is the main source of salinity variations and will be discussed in the next section.

3. One-dimensional formulation of the thermodynamic changes in ice salinity

In a 1D test case, we compare two formulations of θ^s using the same sea ice thermodynamic component. The sophisticated halodynamic module of Vancoppenolle et al. (2007, hereafter referred to as VBF07) would be computationally expensive in a large-scale model with ITD. The second parameterization (SZT) formulates brine entrapment and drainage more simply. First, we briefly describe the thermodynamic component, then the two parameteriza-

[1] LIM = Louvain-la-Neuve sea Ice Model, developed at the Institut d'Astronomie et de Géophysique G. Lemaître, Louvain-la-Neuve, Belgium. In the companion paper (Vancoppenolle et al., 2008, this issue, hereafter referred to as V09), the general features of LIM3 are described and the simulated sea ice characteristics are critically compared to observations. Here, we focus on the sea ice salinity aspects.

tions and, finally, we compare simulations using alternately both parameterizations to observations of landfast sea ice.

3.1. Thermodynamic component

The thermodynamic component used here is the Bitz and Lipscomb (1999) 1D energy-conserving model. Prognostic variables are the ice thickness h, the snow depth h^s and the vertical temperature profile $T(z)$ in the ice-snow system. Temperature variations are computed by numerically solving the heat diffusion equation in 1 layer of snow and 20 layers of sea ice, characterized by their salinity S. In order to represent the salinity effect on heat transfer and storage, through its impact on the sea ice relative brine content, the sea ice thermal properties (i.e., the specific heat c, thermal conductivity k and energy of melting q, defined as the energy required to melt a unit volume of sea ice) depend on S and T. The growth (melt) rates at the interfaces are computed by dividing the heat loss (gain) F by q.

There are two main competing effects of salinity on ice thickness dominated by c and q, k only playing a modest role (Vancoppenolle et al., 2005). First, the increase in specific heat (c) with S favours lower melt rates for more saline ice. Second, the decrease in energy of melting (q) with S yields higher melt rates for more saline ice (Bitz and Lipscomb, 1999).

3.2. Reference salinity model

The reference formulation used to compute the spatio-temporal variations in ice salinity is the halodynamic module of VBF07. It is based on laboratory and field experiments and has been validated against sea ice core data. In this model, the evolution of the sea ice salinity profile is governed by brine explusion (function of the temporal derivative of temperature), gravity drainage (function of the vertical temperature gradient and active when the brine network is open) and flushing (i.e., the percolation of surface meltwater through the open brine network). The relative brine volume $e(z, t)$ is diagnosed as a function of S and T. The brine network is assumed to be interconnected if $e > 5\%$. The boundary condition at the ice–ocean interface specifies the salinity of new ice as a fraction of seawater salinity as indicated by laboratory measurements (Cox and Weeks, 1988) and gives more brine entrapment for larger basal congelation rate.

3.3. Simple parameterization of brine entrapment and drainage

The second parameterization of salinity variations used here is a simplification of the VBF07 halodynamic module, hereafter referred to as SZT. It is designed for use in large-scale 3D models. An equation for the bulk salinity $\overline{S}$ is solved and the shape of the profile is computed as a function of the bulk salinity. This has the advantage that only the bulk salinity has to be transported horizontally and redistributed in thickness space in the 3D model.

Field data (Malmgren, 1927), laboratory experiments (Cox and Weeks, 1975) and 1D simulations with the VBF07 model (Vancoppenolle et al., 2006) indicate that the sea ice desalination can be divided into initial, winter and summer stages. Gravity drainage and flushing dominate winter and summer desalinations, respectively. In addition, salinity data from ice cores drilled in some of the Southern Ocean deep snow-covered regions suggest a salt source at the ice surface associated to snow ice formation (Jeffries et al., 1997; Perovich et al., 2004). Based on this, the equation for bulk salinity includes brine entrapment during basal growth and snow ice formation, gravity drainage and flushing.

Observation of the vertical sea ice salinity profile from ice cores suggests that the shape of the profile is a function of the bulk salinity. At high salinity, the S profile has a C-shape, while at low salinity, the profile has an almost linear shape with low salinity near the surface. This is mainly because of flushing, which affects salinity near the surface (VBF07). In addition, numerical experiments have shown that for mass balance simulation purposes, a linear profile well approximates the realistic, non-linear sea ice salinity profile (Vancoppenolle et al., 2005). Consequently, a profile shape which is function of the bulk salinity is used in the model. At high salinity, the salinity is assumed to be vertically constant. At low salinity, the salinity profile is assumed to be linear, with $S = 0‰$ at the surface. At intermediate salinity, the salinity profile is a linear combination of the linear and vertically constant profiles. For more details on this parameterization, see V09, Section 2.6.5.

3.4. Experimental setup

The 1D model is used to simulate the growth and decay of landfast sea ice at Point Barrow (see Fig. 1), on the northern Alaskan coast (Chukchi Sea site, 2000–2001), using different halodynamic modules (see Table 1). The VBF07 model was already validated at that site against observations of ice thickness, snow depth, salinity and temperature profiles.

The runs were initialized using in situ observations of sea ice physical characteristics (Grenfell et al., 2006) and forced with surface heat fluxes derived from Point Barrow meteorological station data and with a prescribed ocean heat flux (see VBF07, Section 3.2.4, for details).

Five simulations were run using different salinity parameterizations. VBF07 (control run) and SZT are compared with simpler, prescribed salinity profiles. In CW, the salinity is vertically constant and prescribed as a function of ice thickness, using the relation of Cox and Weeks (1974), as in Ebert and Curry (1993). In PR, the vertically varying salinity profile of Schwarzacher (1959), typical

Table 1
Description of the simulations performed with the 1D model.

Experiment	Description
VBF07	VBF07 sophisticated halodynamic module
SZT	Simple parameterization of brine entrapment and drainage
PR	Steady-state, vertically varying salinity profile of Schwarzacher (1959)
CW	Salinity function of ice thickness (Cox and Weeks, 1974)
BK5	Steady-state, isosaline salinity ($\overline{S} = 5‰$)

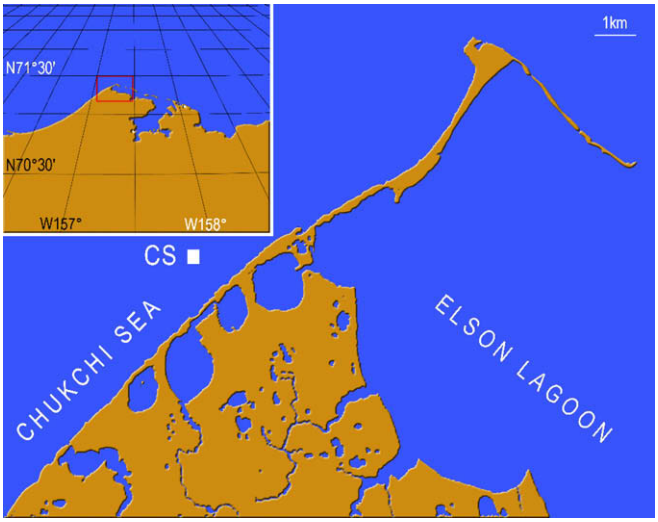

Fig. 1. Map of Point Barrow neighborhood. Chukchi Sea (CS) sampling site is indicated.

of Arctic multiyear (MY) ice, is used, as in Bitz and Lipscomb (1999). Finally, in BK5, an isosaline profile with $S = 5‰$ is used, as in Fichefet and Morales Maqueda (1997) or Zhang and Rothrock (2001).

3.5. Results

Ice salinity. The results of the simulations are shown in Fig. 2. Compared to VBF07, $\overline{S}$ is very well reproduced in SZT (panel b). CW has a correct winter $\overline{S}$, but is not able to simulate flushing. The salinity profile in SZT well approximates the non-linear VBF07 profile (panels e and f). In summer, the simulated near-surface salinity (i.e., taken over the uppermost 50 cm) in VBF07 and SZT are very close (panel c). Desalination in VBF07 is slightly too slow during the first days of summer.

Temperature. The temperature profile is similar in all simulations but PR (panel d). PR is the only case in which the near-surface salinity is low when the melt period starts. The near-surface specific heat is therefore much lower. This yields faster upper ice warming and melt.

Ice thickness. The ice thickness in SZT compares very well with VBF07, which itself agrees best with observations (panel a). The other simulations underestimate the ice thickness by 10 cm.

The difference in ice thickness between PR and VBF07 is due to a larger surface melt rate in PR between days 150 and 160. The warmer upper ice layers in PR during that period suggest that the c effect dominates. The decrease in c associated with low S and high T occurs 10 days later in VBF07 than in PR. After 10 days of melt, the surface melt rates in VBF07 and PR become similar.

In CW and BK5, the differences in ice thickness from VBF07 are due to larger surface melt after day 160. Between days 150 and 160, the near-surface temperature evolves similarly in all three simulations. After day 160, CW and BK5 have a higher near-surface salinity than VBF07. Since the temperature profile is steady and similar in all simulations, only q can play a role here. Due to lower bulk salinity in VBF07 than in CW and BK5, q is larger near the surface, which yields smaller melt rates.

3.6. Summary

In conclusion, VBF07 is well approximated by the simple parameterization SZT. The other parameterizations lead to errors in the simulated salinity, temperature and ice thickness. For the Point Barrow conditions, a time-varying salinity favours lower surface melt rates. In the first 10 days of summer, high near-surface S and c keep the temperature relatively cold near the surface and inhibit the melt. Then, after intense surface drainage, higher q maintains lower melt rates. Similar experiments – not shown here – designed to simulate Arctic MY ice were performed using VBF07 and SZT in a central Arctic configuration.[2] Thicknesses and bulk salinities (transient and equilibrium) are again similar in the two runs. In conclusion, we argue that SZT can be used instead of VBF07 to analyze the impact of sea ice salinity in a large-scale sea ice model.

Moreover, in Vancoppenolle et al. (2006), VBF07 was compared to prescribed, constant profiles in the same central Arctic MY ice configuration. Those experiments indicated the following: taking temporal and vertical variations of ice salinity into account (1) increases basal ice growth, because the energy required to form a unit volume of sea ice is lower and (2) increases surface melt. The second item apparently contradicts the simulations of first year (FY) ice run here, but reflects the fact that for MY, thicker ice, the salinity near the surface is already quite low in early summer, which reduces c near the surface and facilitates surface melt. There are also presumably differences due to snow and radiative forcings.

4. Representation of the salinity distribution in OPA9-LIM3

In this section, we present how the conservation equation for the salinity distribution (4) is solved, using SZT to calculate θ^s, in a large-scale sea ice model.

4.1. LIM3 overview

The ice–ocean model used here is developed in the framework of the ocean modelling system NEMO[3] that combines LIM3, a C-grid, dynamic–thermodynamic sea ice model, with ice thickness, enthalpy, salinity and age distributions and OPA[4] v9.0, a hydrostatic, primitive equation, ocean general circulation model included in NEMO. Hereafter, LIM3 is only briefly described. For more details on LIM3, see V09, Section 2.

The ice in LIM3 is represented as a series of $M = 5$ thickness categories. In each of them, the sea ice cover is vertically divided into $N = 5$ ice layers covered by one layer of snow. Each ice category has its own set of global state variables: the ice concentration, volume per unit area, enthalpy per unit area, salt content and age content, as well as the snow volume per unit area and enthalpy per unit area. Each state variable X has a definite value in all the thickness categories and follows a conservation equation including horizontal transport, transport in thickness space due to ice growth/melt and effects of the thermodynamical and mechanical redistribution processes. The ice momentum equation is solved on a C-grid with an elastic-viscous-plastic rheology (Bouillon et al., 2009). The ice state variables are advected horizontally with the second-order moment conserving scheme of Prather (1986). The thickness distribution formulation is Lagrangian in thickness space and follows Bitz et al. (2001). The transport in thickness space is computed using linear remapping (Lipscomb, 2001). The formulation of the mechanical redistribution is based on the ideas of Thorndike et al. (1975) and Bitz et al. (2001) and includes rafting and porous ridging.

The thermodynamic module of LIM3 includes an exhaustive representation of brine-related processes (see Section 2.6 of V09 for details). The sea ice salt content M^s_m in category m ($m = 1, 2, \ldots, M$) is the extensive variable numerically representing the salinity distribution s in LIM3. It is defined, for each category, as $M^s_m = S^i_m v^i_m$, where S^i_m and v^i_m are the sea ice bulk salinity and volume per unit area in category m, respectively. As for other variables, a conservation equation (i.e., Eq. (4)) is solved. The term θ^s is computed using the simple parameterization SZT described in Section 3.2. The variations in vertical salinity in the N vertical layers $S^i_{m,k}$ ($k = 1, 2, \ldots, N$) are only "seen" by the thermodynamic module. The formation of snow ice introduces salt into the ice cover. Newly forming ice in open water has a salinity given by the salinity-thickness relation of Kovacs (1996). Finally, following earlier studies, the mechanical redistribution function ψ^s is built upon the fundamental ψ^g function (see V09, Section 2.5.4; Eq. (9) in Zhang and Rothrock, 2001; Appendix A of Bitz et al., 2001).

In LIM3, salinity variations affect sea ice thermodynamics as well as ice–ocean salt and freshwater fluxes. The thermal effect of brine inclusions is accounted for through thermal properties that depend on S and T. Sea ice mass source and sink terms include

[2] In those experiments, the seasonal cycle of surface heat fluxes from a central Arctic climatology is repeated over 50 years as model forcing (see Vancoppenolle et al., 2006 for a detail of the setup).

[3] NEMO = Nucleus for European Modelling of the Ocean, developed at LOCEAN, Paris, France.

[4] OPA = Ocean PArallélisé (Madec, 2008).

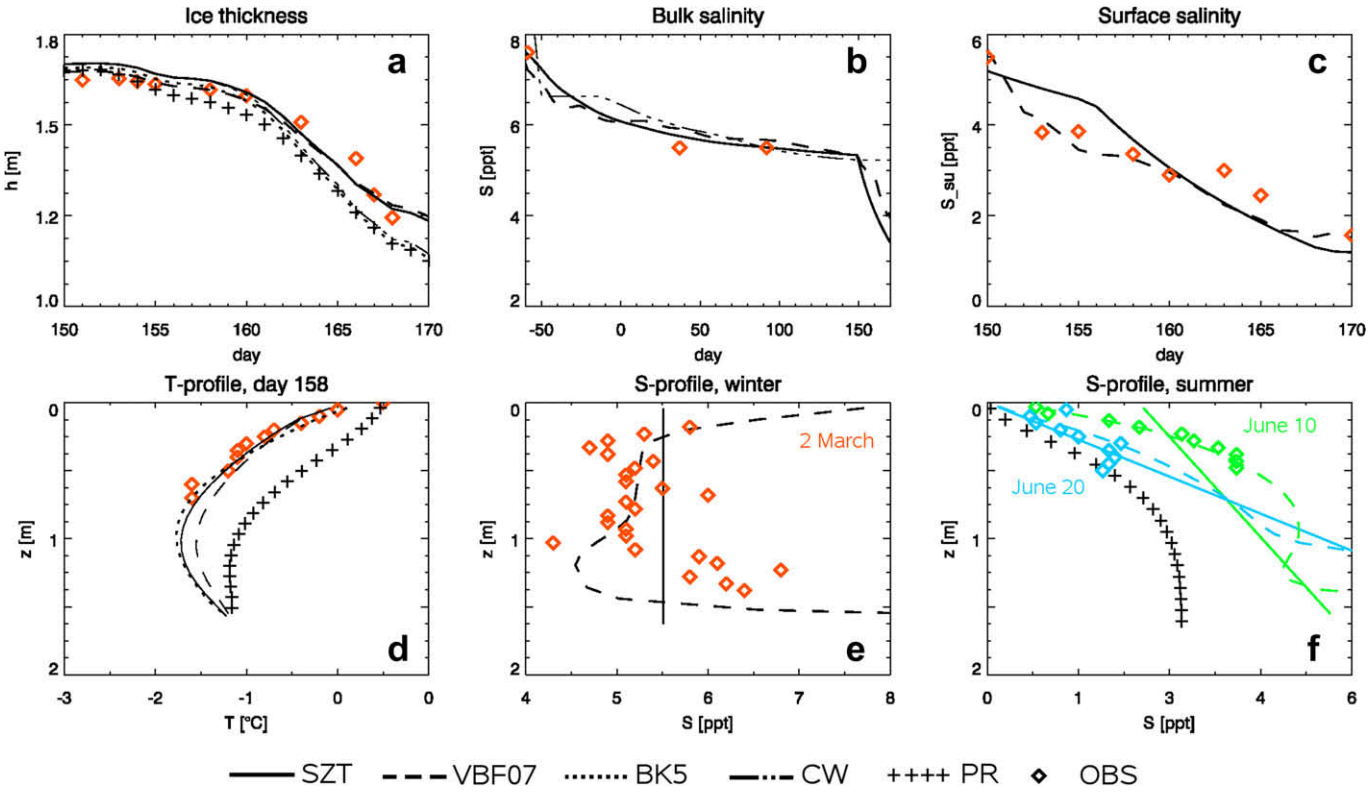

Fig. 2. Impact of the different parameterizations of salinity variations on several simulated features at Chukchi Sea site, 2001. In situ observations from ice cores (courtesy of H. Eicken) are also presented. Temporal evolution of (a) ice thickness, (b) bulk salinity and (c) near-surface salinity (i.e., taken over the uppermost 50 cm of ice); (d) temperature profile on June 8th, (e) winter salinity profile (March 2nd) and (f) early summer salinity profile (June 10th and 20th). Note that on each plot, only the relevant curves are shown: on panels (c), only SZT and VBF07, which compute an ice salinity, are shown; on (d) CW, very similar to BK5, is omitted; on (e) only SZT and VBF07 are shown, on (f) only SZT, VBF07 and PR are shown. (For interpretation of the references to colour in this figure legend, the reader is referred to the web version of this article.)

basal and snow ice growth, growth of new ice in open water as well as basal and surface melt. Vertical growth and decay are determined using a model very close to Bitz and Lipscomb (1999) (see Section 3.1). For more details, see V09, Section 2.6.2. Salt and freshwater exchanges between ice and ocean are represented through the use of the ice–ocean salt and freshwater flux (F^s). F^s, which represents the dilution effect of sea ice on the ocean, can be positive (salt rejection) or negative (freshwater release) and has two components. The first one is the direct effect of ice growth and melt (F^s_{eq}) and accounts for the salinity of growing (or melting) ice. The second one is brine drainage (F^s_b) and is directly related to salinity variations. See V09, Section 2.8 for more details.

4.2. Forcing and experimental conditions

The ocean and sea ice models both run on the same global domain and use the tripolar ORCA2 C-grid with a 2° zonal resolution and a meridional resolution varying from 0.5° at the equator to 2° $\cos\phi$ (see, Timmermann et al., 2005). The simulation (same as in V09) is conducted over the period 1948–2006. Unless otherwise stated, years 1979–2006 are analyzed, for which satellite data are available. Atmospheric forcing fields are a combined data set consisting of NCEP/NCAR daily reanalysis data of 10-m wind speed and 2-m temperature (Kalnay et al., 1996), and monthly climatologies of relative humidity (Trenberth et al., 1989), total cloudiness (Berliand and Strokina, 1980) and precipitation (Large and Yeager, 2004). More details can be found in V09 (Section 3.3). River runoff rates are prescribed using the climatology of Baumgartner and Reichel (1975) combined with a mean seasonal cycle derived from the Global Runoff Data Centre (GRDC) data. Contrary to earlier versions of the model, no salinity restoring is used.

5. Results of the control simulation

In this section, the simulated sea ice salinity field is compared to observations and analyzed. More information on the control simulation (e.g., ice concentration, thickness, ...) can be found in V09, Section 4.

5.1. Mean seasonal cycle of bulk sea ice salinity averaged over the ice thickness categories

5.1.1. Observational data

Many in situ measurements of sea ice salinity have been performed. They were typically obtained from the melt of sea ice cores sections (see, e.g., Malmgren, 1927; Eicken et al., 1991). The simulated salinity field was compared to ice core data. The data set was built from the western literature (see Tables 2 and 3). For each publication, we either took the data from tables or digitized them from plots in the original sources. In the majority of cases, bulk salinity, inter-core standard deviations and the number of drilled cores were available.

These data, collected by different teams, at different places and times, are neither coherent in space nor in time. Furthermore, they are subject to sampling errors due to subfloe-scale variability. Therefore, the following data processing was applied. In order to remove subfloe- and larger-scale spatial variability, average salinities were computed over cores which are coherent in space and time. The inter-core average salinities were then sorted by hemisphere and region. This resulted in 28 (Arctic) and 17 (Antarctic) regional salinity values, corresponding to a total of 1063 individual ice cores. In spite of the processing, the present record remains subject to errors of several origins and could certainly be improved

Table 2
Summary of the Arctic sea ice salinity data used for this study. S is the sea ice mean salinity, σ_S the inter-core standard deviation of S, N is the number of cores. BS stands for Beaufort Sea, AO for Arctic ocean, FS for Fram Strait, BB for Baffin Bay, SV for Svalbard Archipelago (landfast ice), LapS for Laptev Sea and LabS for Labrador Sea.

Month	Year	Season	Sector	S	σ_S	N	References
October–December	22–25	Fall	AO	8.6	3.3	17	Malmgren (1927)
January–March	22–25	Winter	AO	7.8	3.6	9	Malmgren (1927)
May–September	58	Summer	AO	2.2	–	40	Schwarzacher (1959)
August–September	91	Summer	AO	2.1	0.7	66	Eicken et al. (1995)
July–August	94	Summer FY	AO	1.3	0.1	4	Tucker et al. (1999)
July–August	94	Summer MY	AO	2.0	0.4	17	Tucker et al. (1999)
September	22–25	Summer	AO	2.1	0.3	3	Malmgren (1927)
June–July	84	Summer FY	FS	4	–	20	Tucker et al. (1987)
June–July	84	Summer MY	FS	2.1	–	31	Tucker et al. (1987)
March	71	Winter	BS	4.0	1.6	3	Cox and Weeks (1974)
March–April	72	Winter	BS	3.7	0.5	30	Cox and Weeks (1974)
January–May	00-01	Winter–Spring	BS	5.6	0.2	32	Vancoppenolle et al. (2007)
April	69	Spring	BS	6.8	0.4	4	Cox and Weeks (1974)
April	83	Spring	BS	4.7	0.4	5	Tucker et al. (1984)
June	00–01	Summer	BS	3.4	0.3	36	Vancoppenolle et al. (2007)
June–August	58	Summer	BS	1.8	0.6	19	Cox and Weeks (1974)
June–August	98	Summer	BS	2.0	1.7	14	*SHEBA*
September–October	69	Summer	CA	2.2	0.3	9	Cox and Weeks (1974)
October	69	Fall	CA	9.1	2.0	15	Cox and Weeks (1974)
April–May	99	Spring	LapS	3.8	2.0	91	Eicken and Proshutinsky (2005)
May	98	Spring	SV	4–5	–	6	Gerland et al. (1999)
October–November	56	Fall	BB	7.75	–	–	Weeks and Lee (1962)
November–May	77–78	Winter	BB	6	–	13	Nakawo and Sinha (1981)
December–January	55	Fall	LabS	8.5	2.1	21	Weeks and Lee (1958)
January–March	56	Winter	LabS	6.7	0.8	15	Weeks and Lee (1958)
March–May	56	Spring	LabS	4.3	0.8	14	Weeks and Lee (1958)
April	72	Spring	BS	9.6	2.6	24	Cox and Weeks (1974)
February–March	70	Winter	BerS	5.5	0.4	8	Cox and Weeks (1974)

Table 3
Summary of Antarctic sea ice salinity data used in this study. S is the sea ice mean salinity, σ_S the standard deviation of S, N is the number of cores. WP stands for West Pacific sector, I for Indian sector, RS for Ross Sea, BeS for Bellingshausen Sea and WS for Weddell Sea.

Month	Year	Season	Sector	S	σ_S	N	References
April	93	Fall	WP	7.6	1.9	18	Worby et al. (1998)
August	99	Winter	WP	13.0	4.1	43	V. Lytle (unpub.)
October	91	Spring	WP	5.5	1.8	4	Worby et al. (1998)
September	94	Winter	I	6.5	2.0	33	Worby et al. (1998)
November	91	Spring	I	5.7	1.3	15	Worby et al. (1998)
November	92	Spring	I	6.7	3.3	24	Worby et al. (1998)
July–August	01	Winter	BeS	7.1	1.1	20	Perovich et al. (2004)
August–November	93–94	Winter	BeS	5–6	–	13	Jeffries and Porter (1995)
October–November	80	Spring FY	RS	5.9	0.7	26	Gow et al. (1998)
November	04	Spring MY	RS	3.86	2.17	13	Eicken (unpub.)
September–October	89	Winter–Spring FY	WS	6.0	1.2	22	Eicken (1998)
September–October	89	Winter–Spring MY	WS	4.8	1.4	9	Eicken (1998)
October–November	88	Spring	WS	4.2	0.3	8	Eicken et al. (1991)
May–December	86–89	Winter–Spring	WS	6	–	129	Eicken (1992)
December	04	Summer	WS	5.5	1.0	14	Tison et al. (2008) Hellmer et al. (2006)
February–March	80	Summer–Fall FY	WS	4.5	0.9	62	Gow et al. (1987)
February–March	80	Summer–Fall MY	WS	3.4	0.5	14	Gow et al. (1987)

by adding more data. The large-scale pattern shown by the data can however be considered as reliable thanks to the already large amount of data compiled.

5.1.2. Comparison model-observations

For several regions in both hemispheres, each observed salinity was plotted versus the corresponding mean sampling month, independently of the sampling year, and compared with the corresponding mean salinity (weighted over the thickness categories) taken from the seasonal 1979–2006 model climatology (see Fig. 3). The regions considered in the Northern Hemisphere (hereafter referred to as NH) are the Arctic Ocean, its peripheral seas (Kara, Laptev, East Siberian, Chukchi and Beaufort Seas) and the outer Arctic, which gathers the remainder of the ice-covered regions of the NH. The Arctic region corresponds to the Arctic Ocean and its peripheral seas.

The model-data agreement is generally good, though there are a few data points in the NH characterized by a very high salinity for which the model-data agreement is poor. For most of those points, the model-observation discrepancy error is presumably due to the low statistical representativity of the observed value. For example, the high salinity March–April point in the NH (see top of Fig. 3a, data point from Cox and Weeks, 1974) is typical of newly formed thin ice, whereas the simulated value – averaged over thickness categories – is dominated by thick ice.

Field studies report significant differences between Arctic and Antarctic sea ice salinities (see, e.g., Gow and Tucker, 1990) that are simulated by the model. First, both data and model indicate that sea ice is more saline in the Southern Hemisphere (SH) than in the NH. This is because, in the SH, (1) the relative contribution of young – and therefore more saline – ice, is higher, (2) the amount of surface melt and flushing is much lower and (3) the

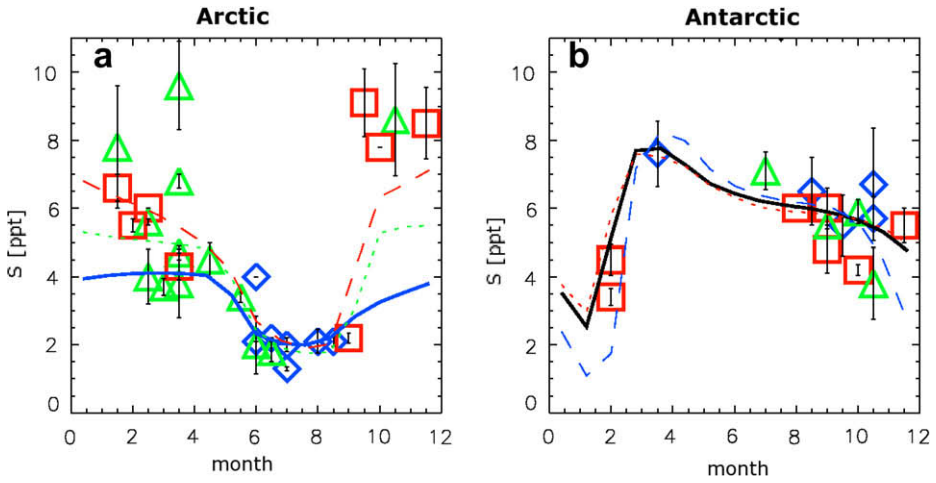

Fig. 3. Simulated and observed 1979–2006 mean seasonal cycle of ice salinity in several regions of the Arctic (a) and Antarctic (b), control run (referred to as SZT-IO). The model means take into account the volume-weighted contributions of the ice thickness categories. The observations are inter-core means computed from different field campaigns (see text for details). Regions for model values in the Northern Hemisphere (NH) are: Arctic Ocean (solid blue), peripheral seas (green dot, see text for definitions) and outer Arctic (red dash). For observations, regions are: Arctic Ocean and Fram Strait (blue diamonds); peripheral seas (green triangles) and outer Arctic (red squares). Regions for model values in the Southern Hemisphere (SH) are: global Southern Ocean (black solid), West Pacific sector (blue dash) and Weddell Sea (red dots). For observations, regions are: West Pacific and Indian sectors (blue diamonds), Weddell Sea (red squares) and Ross, Amundsen and Bellingshausen Seas (green triangles). (For interpretation of the references to colour in this figure legend, the reader is referred to the web version of this article.)

contribution of snow ice formation, which traps large amounts of salt, is higher (see V09) than in the NH.

Fig. 3 reveals that there is a large amplitude seasonal cycle of ice salinity in both hemispheres, characterized by a maximum in fall and a minimum in summer. The annual minimum salinity thus occurs when the ice is the oldest (summer). This minimum reaches around 2‰ in the NH and 4‰ in the SH. The seasonal maximum salinity takes place when the abundance of newly formed, saline ice is the largest (fall).

5.2. Ice salinity distribution in thickness space

The second model validation test that was performed is the comparison of salinity distribution in thickness space with the observations of Cox and Weeks (1974). Cox and Weeks' relations were compiled from NH data and show a winter decrease in ice salinity with thickness. In summer, ice has salinity around 2‰ for all ice thicknesses.

The seasonal cycle of the salinity distribution in thickness space is shown in Fig. 4. In the NH, the model agrees well with the Cox and Weeks' relations. The salinity distribution is characterized, on the one hand, by large differences in winter, with young, thin ice being more saline than old, thick ice, and on the other hand, by an isosaline ice cover in summer. In addition, the winter NH simulated salinity and age are strongly correlated (−0.78). In the SH, variations in ice salinity with h are lower. The SH simulated age-salinity correlation is low, because of the low surface melt and flushing, which prevents the formation of a low salinity MY ice cover.

5.3. Geographical variations of ice salinity

Fig. 5 depicts the geographical variations in mean ice salinity simulated by OPA9-LIM3. In the NH, the regional variations reflect the FY-MY contrast, with larger values in the seasonal ice zone (SIZ), associated with young ice, and lower values in the perennial ice zone (PIZ), associated with old ice. In the peripheral seas, intermediate salinities are found and reflect the mixture of young and old ice. In contrast to the other Arctic regions, the simulated winter sea ice salinity in the Baltic Sea lies within

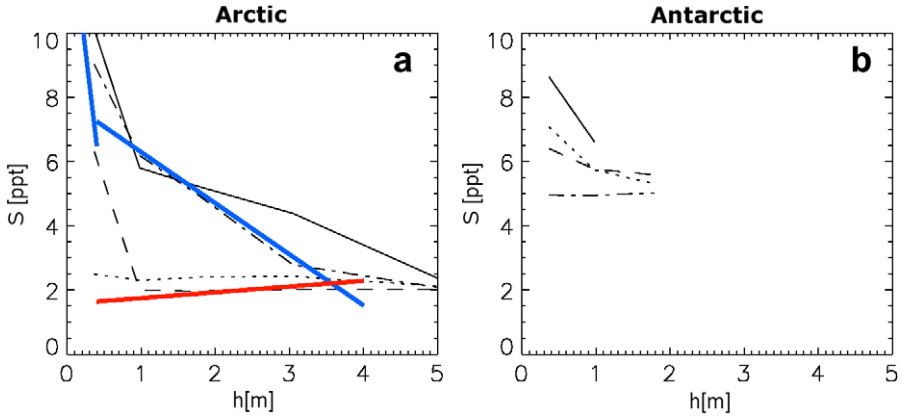

Fig. 4. Simulated mean bulk salinity S (‰) in function of ice thickness h (m) averaged over the Arctic (a) and the Antarctic (b) in March (solid), June (dot), September (dash) and December (dash-dot), SZT-IO run. On the left panel, the Cox and Weeks (1974) $S - h$ relations for winter (blue) and summer (red) – which were derived from cores in the Arctic region – are depicted. (For interpretation of the references to colour in this figure legend, the reader is referred to the web version of this article.)

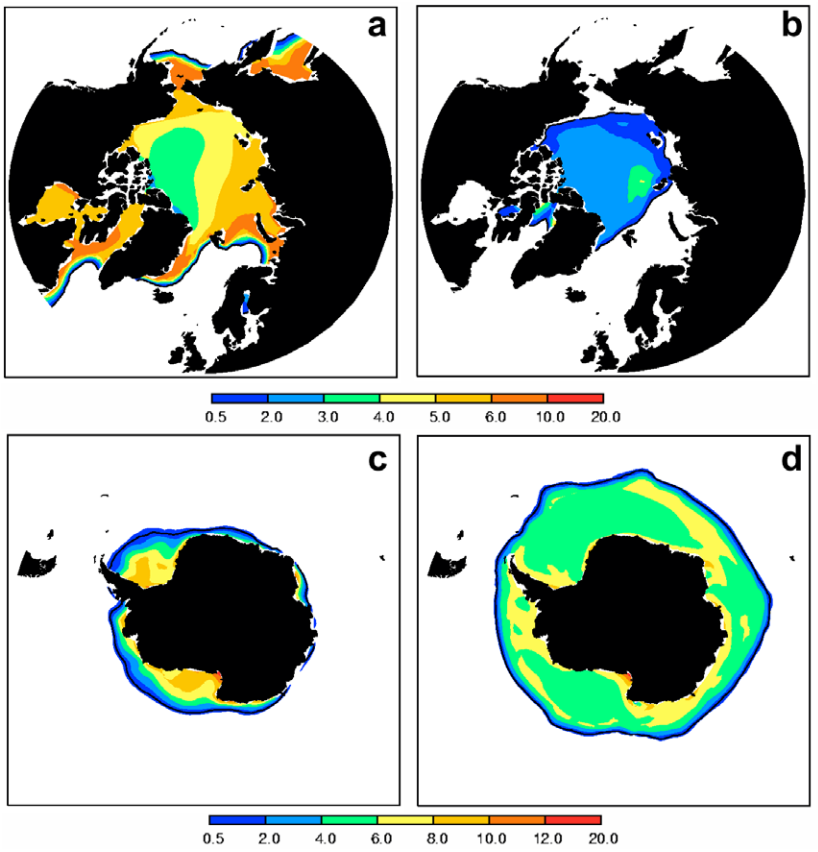

Fig. 5. Simulated spatial distributions of mean sea ice salinity (‰) in the NH, March (a) and September (b), and in the SH, March (c) and September (d), 1979–2006, SZT-IO run. The means take into account the weighted contributions of the ice thickness categories, but exclude open water.

0–2‰. Granskog et al. (2004) reported similar values (0–1.5‰). Moreover, sea surface salinity ranges from 6‰ to 8‰ in the Baltic Sea. Therefore, fractional entrapment of brine during growth leads to much lower salinities, which is well reproduced by the model. In the SH, the regional variations in ice salinity are relatively small compared to the Arctic, though salinity is higher than average where ice forms intensively, i.e., along the ice edge and in coastal polynyas in the Weddell and Ross Seas as well as along East Antarctica.

6. Sensitivity experiments

In order to investigate the impact of salinity variations on the simulated sea ice and upper ocean physical characteristics, we run several sensitivity experiments which are summarized in Table 4. In most models, the ice salinity is considered as a constant, only used to compute the salt/fresh water fluxes at the ice–ocean interface (e.g., Fichefet and Morales Maqueda, 1997). In some of them, the impact of sea ice salinity on ice thermodynamics has been considered either through a vertically varying salinity profile, fixed in time (e.g., Bitz et al., 2001; Hunke and Lipscomb, 2004), or through an isosaline profile varying in time (e.g., Schramm et al., 1997). The latter case has been shown to misrepresent ice melt in summer in Section 3. Therefore, it is not included in the following sensitivity experiments.

Table 4
Description of the simulations performed with OPA9-LIM3.

Experiment	Description
SZT-IO	Prognostic ice salinity used
SZT-I	Prognostic ice salinity used in thermodynamic computations only
BK5	Prescribed, vertically constant salinity ($S = 5$‰)
PR	Steady-state, vertically varying salinity profile (Schwarzacher, 1959)

In SZT-IO (control simulation analyzed above), (1) the temporal and vertical variations in ice salinity are included and affect the sea ice thermodynamic processes. (2) The ice–ocean salt flux F_b^s due to brine drainage is applied. (3) The ice–ocean salt/freshwater flux due to ice growth/melt F_{eq}^s is computed using a varying salinity. If the ice is growing, this salinity depends on the formation mechanism (i.e., new ice formed in open water, at the ice base and through snow ice formation). If the ice is melting, this salinity corresponds to the salinity of the melting ice layer.

In SZT-I, (1) the variations of ice salinity are included in the sea ice thermodynamic computations. (2) F_b^s is set to 0. (3) F_{eq}^s is computed using a prescribed salinity ($S = 5$‰) if ice grows or melt. Though this run is not salt-conserving, its interest is to isolate the effects of salinity variations on sea ice thermodynamics. In contrast, the impact of salinity variations on the total ice–ocean salt flux (F^s, hereafter referred to as *ice–ocean salt flux*) and their influence on ocean and sea ice, through oceanic feedbacks, are excluded.

In BK5, the ice is supposed isosaline with $S = 5$‰ in the sea ice thermodynamic computations as well as in the computation of F^s, as in Fichefet and Morales Maqueda (1997) or Zhang and Rothrock (2001).

In PR, the steady-state, vertically varying profile of Schwarzacher (1959), typical of central Arctic MY ice, is used in the sea ice thermodynamic computations and the corresponding vertically-averaged salinity ($S = 2.3$‰) is used to compute F^s. Some authors, as Bitz et al. (2001), use such a setup, though the mean salinity

used to compute the ice–ocean salt flux is different from the mean of the profile.

The three sensitivity runs describe above are restarted from the control run SZT-IO, on December 31, 1969.

6.1. Northern hemisphere

In the NH, most of the changes are due to the effect of salinity on the thermal properties of sea ice. Therefore, regarding NH sea ice characteristics, the simulations SZT-IO and SZT-I are similar, while BK5 and PR differ. As the Arctic Ocean is quite stable vertically, the changes in the ice–ocean salt flux and in oceanic characteristics are too small to induce significant feedbacks on sea ice. In light of these remarks, in the NH, the discussion is focused on SZT-IO and BK5. Significant differences in PR and SZT-I are only reported when necessary.

6.1.1. Sea ice characteristics

Ice thickness. Ice is significantly thicker in SZT-IO than in the three sensitivity runs (see Fig. 6). The most remarkable differences in mean ice thickness h between SZT-IO and BK5 are found north of the Canadian Archipelago and Greenland (10–50 cm) and in the Beaufort Gyre (5–15 cm). Differences between SZT-IO and PR are even larger, lying in the 10–50 cm range in most of the Arctic Ocean and from 50 to 100 cm north of the Canadian Archipelago. Differences in h between SZT-IO and SZT-I are within 10 cm. Simulating salinity variations in SZT-IO reduces the ice thickness bias between model and submarine observations (Rothrock et al., 2008). The improvement reaches 3 cm compared to BK5 and 30 cm compared to PR over 1975–2000 (see Table 5 for details).

Sea ice mass balance. Differences in ice thickness between the 4 runs are due to changes in the sea ice thermal properties that affect sea ice growth and melt. Ice grows more in SZT-IO than in BK5, but also melts more. As the differences in ice growth dominate, ice is slightly thicker in SZT-IO. Similarly, ice is thicker in SZT-IO than in PR, as a result of larger ice growth. However, because SZT-IO and PR have similar melt rates, the differences in h are larger than when comparing SZT-IO and BK5.

On an annual basis, the ice growth in SZT-IO is 5% larger than in BK5. In SZT-IO, salinity of new ice forming at the ice base and in open water is more than the 5‰ used in BK5, which reduces q (the energy required to form a unit volume of sea ice) and increases ice growth for a given heat loss. The more ice growth in SZT-IO is due, in the PIZ, to more ice formation at the ice base and in the SIZ, to more new ice formation in open water.

The annual amount of sea ice melt is 11% larger in SZT-IO than in BK5, 80% of the changes being due to basal melt, and the remainder to surface melt (in the PIZ). First, in summer, S near the ice base is smaller in SZT-IO than in BK5, which reduces the specific heat c and, in turn, apportions more heat to melting at the ice base rather than to internal warming. In addition, in early summer, as thin ice melts more rapidly in SZT-IO, more solar radiation penetrates into the upper ocean, which increases the oceanic heat flux by 4 W/m^2. Second, in summer, S near the surface is nearly zero in SZT-IO,

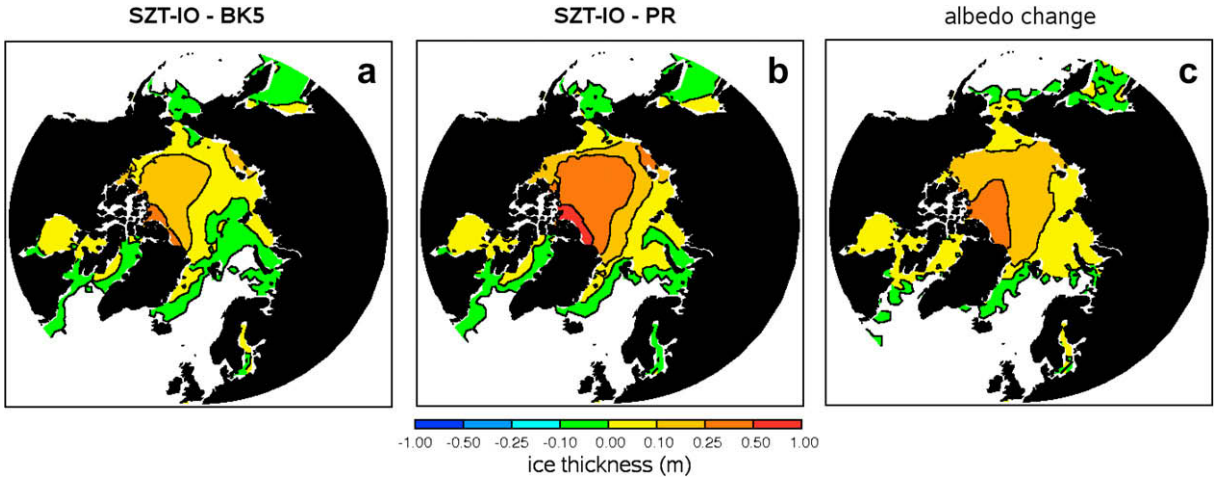

Fig. 6. 1979–2006 differences in March sea ice thickness between (a) SZT-IO and BK5; and (b) SZT-IO and PR, for the NH. (c) Difference in ice thickness from SZT-IO in a run with summer bare ice albedo increased by 10%.

Table 5
Statistics for the control and sensitivity runs. $V(10^3\ km^3)$ and $E(10^6\ km^2)$ are the total ice volume and extent over the hemisphere of interest, respectively. $\Delta h_{ULS}(m)$ is the biais in ice thickness between simulated and observed values. The observed ice thickness is derived from upward-looking sonar (ULS) observations of ice draft (Rothrock et al., 2008). See V09, Section 4.3.1 for details on the procedure. $C_{mod-obs}$ is the correlation coefficient between the simulated and observed monthly mean anomalies of ice extent. Observations of ice coverage are derived from passive microwave observations (Comiso, 2007).

Source	Hemisphere	V_{min}	V_{mean}	V_{max}	$\Delta h_{mod-ULS}$	E_{min}	E_{mean}	E_{max}	$C_{mod-obs}$
DATA	N	–	–	–	–	5.9	12.0	16.3	–
SZT-IO		11.8	18.8	25.1	−0.55 ± 1.04	5.8	10.9	14.4	0.74
SZT-I		12.0	18.9	25.2	−0.53 ± 1.01	5.9	10.9	14.4	0.73
BK5		12.1	18.5	24.4	−0.58 ± 1.00	6.0	10.9	14.5	0.72
PR		10.4	17.2	23.2	−0.83 ± 0.98	5.8	10.9	14.5	0.73
DATA	S	–	–	–	–	3.3	11.9	18.8	–
SZT-IO		0.2	4.8	8.9	–	1.0	11.8	19.3	0.65
SZT-I		0.1	3.4	6.4	–	0.4	10.1	17.4	0.63
BK5		0.1	3.8	7.3	–	0.5	10.9	18.6	0.62
PR		0.1	3.6	6.8	–	0.5	10.7	18.5	0.64

which largely reduces c compared to $S = 5‰$ in BK5 and facilitates melting. For this reason, SZT and PR have comparable surface melt rates. For a more detailed discussion of the impact of sea ice thermal properties on the rates of ice growth and melt, see Vancoppenolle et al. (2005).

Ice volume, area and concentration. Differences in ice thickness induce differences in NH ice volume (see Table 5). As ice grows more rapidly in SZT-IO than in BK5, the seasonal maximum of ice volume is 1.5% larger, but as the ice melts also more rapidly, the minimum ice volume differs only by 0.8% between SZT-IO and BK5. Similarly, as ice grows more rapidly in SZT-IO than in PR and as both simulations melt ice at about similar rates, the ice volume in SZT-IO is on average 11% larger than in PR.

Differences in ice concentration between runs are rather small. In winter, differences are located in the marginal ice zones (MIZ) and show qualitatively similar patterns for the three sensitivity runs, including SZT-I. We only report here the main differences. In winter, in the Labrador Sea, ice concentration in SZT-IO is higher by about 0.1 compared with BK5, which is associated with a less intense convective activity in SZT-IO (see Section 6.1.3 for a discussion of changes in the oceanic circulation). Moreover, the ice tongue along Greenland is narrower, with ice concentration up to 0.05–0.1 lower in SZT-IO than in BK5, due to a shift to the west of the Greenland Sea deep convection site. In summer, due to the more rapid melt of thin ice in SZT-IO, ice concentration is 0.05–0.1 lower than in BK5. Largest (lowest) differences are found where ice melts the most (least), i.e., on the Siberian shelf (along the Canadian coast). Finally, the resulting differences in total ice extent between the four simulations are small, within 0.2×10^6 km^2 (see Table 5).

6.1.2. Ice–ocean interactions and characteristics of the ocean

Storage of freshwater and salt in sea ice. First, we investigate how the representation of ice salinity affects the sea ice freshwater and salt contents and their potential impact on the ocean. In a given region R, the sea ice freshwater content C^i_{fw} (kg H_2O) can be defined as

$$C^i_{fw} = \rho_i \int_R \int_0^\infty hg(h)\,dh\,dR, \tag{6}$$

where ρ_i is the sea ice density. The sea ice salt content C^i_s (kg NaCl) is

$$C^i_s = \rho_i \int_R \int_0^\infty hg(h)\frac{S}{1000}\,dh\,dR \tag{7}$$

and the sea ice dilution potential $C^i_{dil} = C^i_{fw}S^w/1000 - C^i_s$, where S^w is the seawater salinity. C^i_{dil} is a measure of the ocean dilution effect if all ice melted, accounting for both freshwater and salt contents in sea ice.

In Fig. 7, the mean seasonal cycle of these three diagnostics for the NH is depicted. For freshwater content, differences are due to ice volume, while for salt content, they are due to both ice volume and salinity. Though, on annual average, differences in freshwater contents between SZT-IO and BK5 are within 1%, the salt content is overestimated by 25% in BK5, with maximum differences in summer. Consequently, in SZT-IO, the sea ice dilution potential is 5% higher than in BK5. The change in the dilution potential is small compared to salt content, which is due to rather small sea ice salinity in regard to oceanic values. Moreover, compared to SZT-IO, PR underestimates the freshwater and salt contents by 8% and 42%, respectively. As differences tend to counterbalance each other, PR consequently underestimates the sea ice dilution potential by 4% compared to SZT-IO. Finally, though the changes in the NH sea ice dilution potential seem relatively small, they have a significant impact on the ocean (see below).

Ice–ocean salt and freshwater fluxes. Now, we describe how the ice–ocean salt and freshwater fluxes differ in the present simulations. Applying a 1D sea ice model to a landfast ice case study, Vancoppenolle et al. (2005, 2006) showed that the differences in ice–ocean salt flux are dominated by differences in growth/melt rate, but also that the relatively high salinity of growing ice at the base, typically 6–10‰, reduces the ice–ocean salt flux. In the simulations presented here, this effect is enhanced due to the contribution of highly saline ice growing in open water (up to 13‰).

For this reason, during the ice growth season, averaged over the NH, the total ice–ocean salt flux (F^s) is 7% smaller in SZT-IO than in BK5. Differences are the largest in regions of strong ice production (e.g., over the Siberian shelf). In summer, the most important process is the release of freshwater through sea ice melting. Due to larger melt in SZT-IO compared to BK5, the absolute value of F^s (negative) is 6% larger. Furthermore, in early summer, salt is rejected into the ocean through brine drainage (flushing). The latter salt release is weak compared to the dilution due to melting but significant: the mixed layer in early summer is 3 m deeper in SZT-IO than in BK5. While this could be a model analog for the convection plumes that were observed in the upper ocean under early summer melting sea ice near Spitsbergen (Widell et al., 2006), this seems not to have any significant large-scale impact in the present simulations.

Characteristics of the upper ocean. In SZT-IO, waters are fresher at the surface (by 0–0.8‰, average over 1979–2006) and slightly more saline at 200 m depth (by 0.1‰) than in BK5 (Fig. 8), which suggests that the reduced salt flux at the surface due to sea ice growth stabilizes the water column and reduces vertical mixing. The main differences in sea surface salinity (SSS) are located in the intense ice formation zones: on the East Siberian shelf (0.5–0.8‰) and in the Hudson Bay (0.15–0.25‰). The fresher waters formed on the Siberian shelf recirculate into the Beaufort Gyre, where surface waters are also fresher (0.3–0.5‰). In the remainder of the Arctic Ocean, differences are smaller than 0.2‰. On the East Siberian shelf, more than half of the differences can be attributed to the direct effect of varying salinity on F^s. Compared to the Polar Science Center Hydrographic Climatology (PHC, Steele et al., 2001), SZT-IO reduces the bias in SSS on the Siberian shelf, in Chukchi and Beaufort Seas, as well as along the northern coast of Greenland.

The largest changes in mixed layer depth[5] are found near the North Atlantic deep convection sites. First, associated with small changes in the position of the Jan Mayen Current, the Greenland Sea convection site (between Iceland and Svalbard) is slightly displaced to the west in SZT-IO compared to BK5 and PR. The Labrador Sea convection site – displaced to the South – is comparatively more affected. As the the mixed layer is similar in SZT-I and BK5, changes must be due to the direct impact of salinity variations on the ice–ocean salt flux. In fall, during the preconditioning of upper seawater for deep convection, there is the same amount of new ice formed in the Labrador Sea and Baffin Bay in SZT-IO and in BK5. What changes in SZT-IO is the associated salt rejection to the ocean, which is 5–10% smaller than in BK5. Thus, the water column is fresher and more stable in SZT-IO than in other runs, which in turn displaces convection to the South. The position of both deep convection sites slightly better match observations in SZT-IO (Marshall and Schott, 1999; de Boyer Montégut et al., 2004). Moreover, changes in deep convection in the Labrador Sea are associated with changes in oceanic currents, but our runs are too short to draw firm conclusions on the impact of salinity variations on the global oceanic circulation. Finally, in the Arctic Ocean, because of the strong stratification, the changes in

[5] Unless otherwise stated, simulated mixed layer depth is diagnosed using a density-based criterion, with a threshold value of 0.01 kg/m^3.

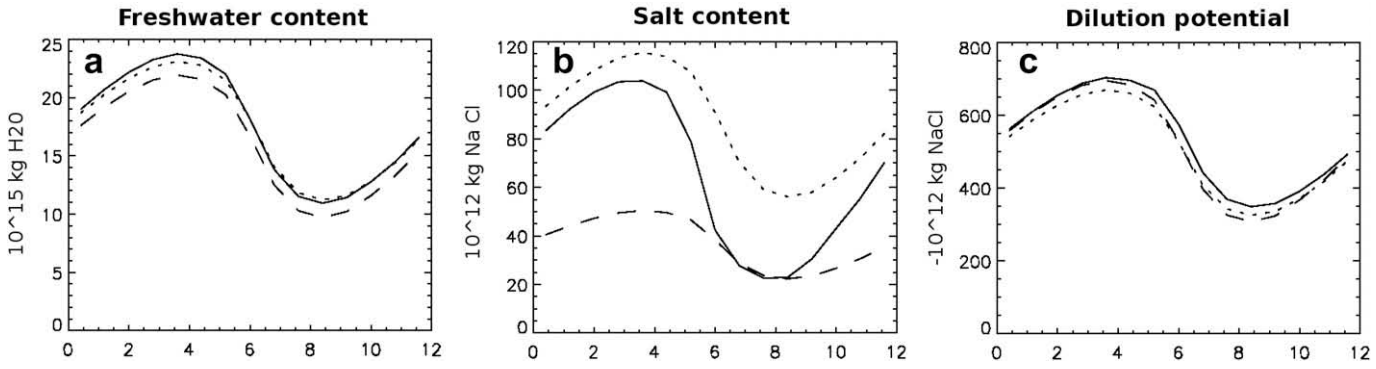

Fig. 7. Mean 1979–2006 seasonal cycle of the total sea ice freshwater content (a), salt content (b) and dilution potential (c) as defined in Section 6.1.2 for the entire NH. Solid lines correspond to SZT-IO, dotted lines to BK5 and dashed lines to PR. Since SZT-I does not conserve salt, it makes no sense to show the associated diagnostics.

SSS are not large enough to significantly affect the simulated mixed layer depth.

6.2. Southern hemisphere

In contrast to the NH, variations in sea ice salinity in the SH have an important impact on sea ice and upper ocean through changes in ice–ocean interactions. In the Southern Ocean, the water column is typically less stable and therefore more sensitive to changes in the buoyancy forcing from sea ice growth/melt than in the NH, which easily triggers feedbacks. In particular, changes in the ice–ocean salt flux are important, which is confirmed by differences between SZT-IO and SZT-I, that are much larger in the SH than in the NH. Qualitatively, the results of the three sensitivity runs BK5, PR and SZT-I are similar. As the results of BK5 and PR are also quantitatively close, only BK5 will be mentioned in the following discussion.

6.2.1. Sea ice characteristics

Ice concentration and thickness. As a result of the representation of ice salinity variations, on annual average, ice concentration is generally higher in SZT-IO compared to the other sensitivity runs, except slightly negative differences in the Indian and West Pacific sectors (see Fig. 9, panel a). The largest differences are found in the central Weddell Sea (0.1–0.5, spring) and close to the ice edge in the Weddell, Bellingshausen, Amundsen and Ross Seas (0.1–0.2, winter). The geographical distribution of the differences is qualitatively similar among the three sensitivity runs. In addition, sea ice is the thickest in SZT-IO (see Fig. 9, panel b), with a maximum difference just after melt onset in spring. Again, differences are the largest in the central Weddell Sea (10–50 cm), are slightly smaller in the Ross Sea (5–25 cm), extend along the coast of Adélie Land and are rather weak along the coast of East Antarctica (5–15 cm). Both in terms of thickness and concentration, model-observation agreement is the best in SZT-IO, though ice is still too thin in SZT-IO compared to observations (see, e.g., Worby et al., 2008 and V09).

Ice area and volume. Though not perfectly simulated, the seasonal cycle of ice extent is represented optimally in SZT-IO (see Table 5). In particular, due to thicker ice in SZT-IO, the mean winter ice extent is 4–10% higher than in the sensitivity runs. Correlation between model and observed monthly mean anomalies of SH total ice extent are slightly higher in SZT-IO than in the other simulations. Moreover, the total SH ice volume is 18–28% higher in SZT-IO, mostly due to a higher maximum.

Sea ice mass balance. Differences in ice thickness and concentration between the runs are due to changes in the ice–ocean salt flux that feedback on sea ice through the oceanic heat flux and basal melt. Though the mean seasonal cycles of the main terms of tendency for ice thickness are shown only for the Weddell Sea (see Fig. 10, panels a and b) – where the differences among the runs are the largest and contribute the most to differences in SH ice volume – the whole Southern Ocean pattern is discussed hereafter.

The process that dominates the change in sea ice mass balance is basal melt: it is lower in SZT-IO, which results in higher h in SZT-IO compared to the sensitivity runs. Lower basal melt in SZT-IO is caused by ocean feedbacks, as indicated by the large differences between SZT-IO and SZT-I. Due to the high interactive salinity of

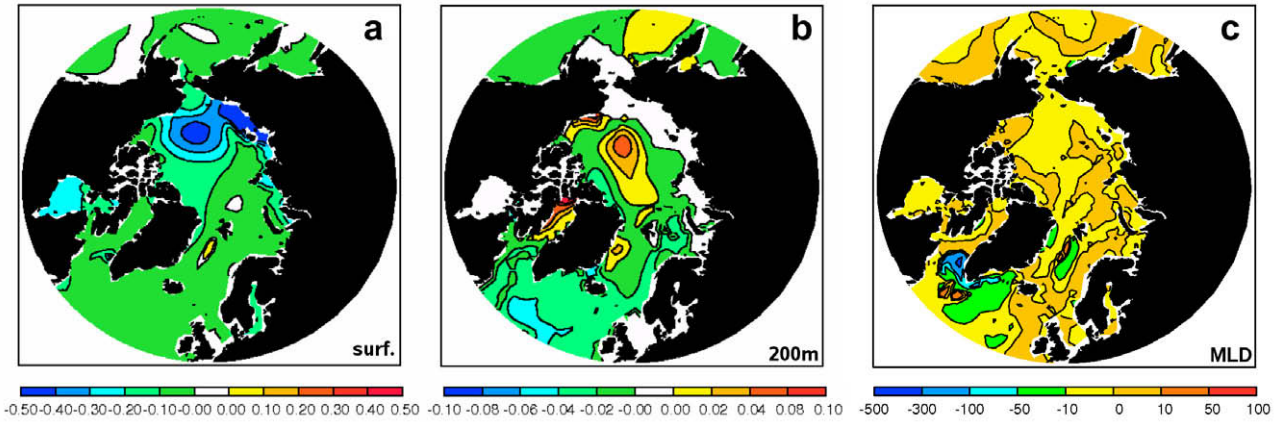

Fig. 8. SZT-IO – BK5 1979–2006 differences in oceanic salinity (March) in the NH (a) at the surface and (b) at 200 m depth. (c) Same, but for mixed layer depth, winter.

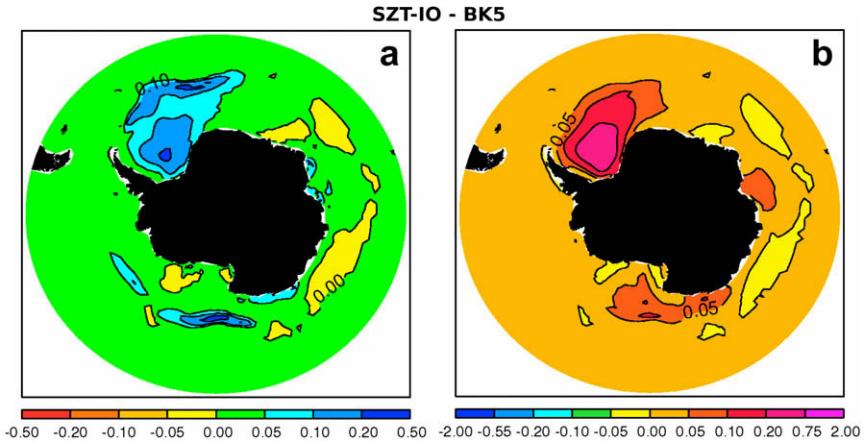

Fig. 9. Annual mean 1979–2006 SZT-IO – BK5 differences in (a) ice concentration and (b) thickness (m) in the SH.

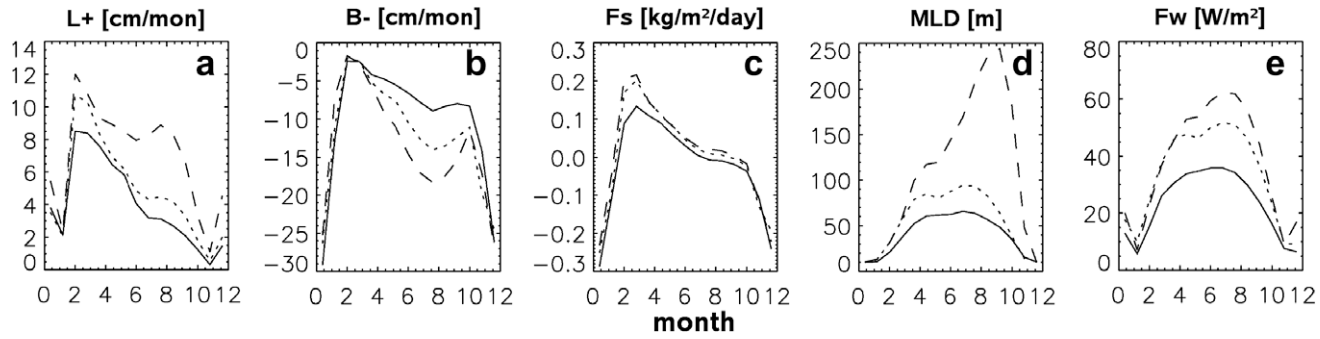

Fig. 10. Mean 1979–2006 seasonal cycle, averaged over the Weddell Sea, of (a) production of new ice in open water, (b) basal melt, (c) ice–ocean salt flux, (d) mixed layer depth and (e) oceanic heat flux; model runs SZT-IO (solid), BK5 (dots) and SZT-I (dash). Ice production/melt terms are expressed as tendencies for ice thickness (cm/month).

new ice, less salt is rejected during ice growth in SZT-IO than in the sensitivity runs. In turn, in SZT-IO, the ocean is more stable, characterized by a shallower mixed layer and a lower oceanic heat flux. Hence, basal melt is 6 (21)% smaller than in BK5 (SZT-I). The differences are magnified in SZT-I because, due to lower q, ice formation is larger in SZT-I, which further enhances salt rejection. Finally, as surface melt is rather small in the Southern Ocean (see, e.g., V09, Section 4.3.3), changes in surface melt do not have a significant impact.

Since, in SZT-IO, the early fall sea ice extent and winter ice concentration are larger than in BK5, the total amount of ice grown in open water is smaller. Again the effect is magnified in SZT-IO: because of tremendous ice melt in summer, new ice growth is 37% weaker in SZT-IO than in SZT-I. In SZT-IO, as the ice is more compact, ice grows rather at the ice base. Basal growth is 5% (9%) larger in SZT-IO than in BK5 (SZT-I).The differences are due not only to smaller q in SZT-IO, caused by higher new ice salinity, but also because of the oceanic heat flux, which is 11–15% weaker in SZT-IO compared to the sensitivity runs. Snow ice growth is 3–5% lower in SZT-IO than in the three sensitivity runs. This is particularly true in the Weddell Sea. In SZT-IO, ice is thicker than in the sensitivity runs and, hence, negative freeboards are less frequent. Due to reduced ice–ocean salt flux, lower oceanic heat flux and smaller q, new ice formation near the ice edge is the highest in SZT-IO.

Note that basal melt occurs all along winter in the model. This occurs because of the combination of the large magnitude of the oceanic heat flux (see V09) and of the synoptic weather variability, which is characterized by the alternance between the transport of cold (warm) air masses from the continent (ocean). Though, in reality, basal ice growth/melt can only work alternately, they artificially seem to occur simultaneously in the climatological monthly means.

6.2.2. Ice–ocean interactions and characteristics of the ocean

Storage of freshwater and salt in sea ice. We first assess what is the potential dilution impact of the sea ice on the ocean. Due to the higher sea ice volume in SZT-IO, the SH sea ice freshwater content (see Fig. 11) is 20 (25)% larger than in BK5 (PR). Due to higher sea ice volume and higher mean salinity in SZT-IO, on annual average, the SH sea ice salt content is 34 (72)% larger than in BK5 (PR). The differences in freshwater content dominate the differences in salt content, and therefore BK5 (PR) underestimates the sea ice dilution potential by 16 (15)%. As in the NH, differences in salt content dominate between BK5 and PR. In conclusion, due to higher sea ice volume, the sea ice dilution potential is the highest in SZT-IO, which favours fresher upper ocean surface in summer and a more stable stratification in early winter.

Ice–ocean salt flux. The high interactive salinity of new ice reduces the ice–ocean salt flux in SZT-IO: integrated over the growth season, the total ice–ocean salt flux (F^s) in SZT-IO is 12 (36)% lower than in BK5 (SZT-I) (see Fig. 10, panel c). Again, the change is mostly attributed to the ice–ocean salt flux due to ice growth (F^s_{eq}). Finally, in summer, due to the higher dilution potential in SZT-IO, the fresh water flux due to ice melt is larger by 9–13% than in the sensitivity runs.

Characteristics of the upper ocean. In the SH, due to the higher sea ice dilution potential, surface waters are 0–0.25‰ fresher in SZT-IO than in the sensitivity runs (see Fig. 12, panel a). Differences among runs are maximum in spring and summer in the zones where ice melts the most (i.e., Weddell Sea and off East Antarctica). Lower

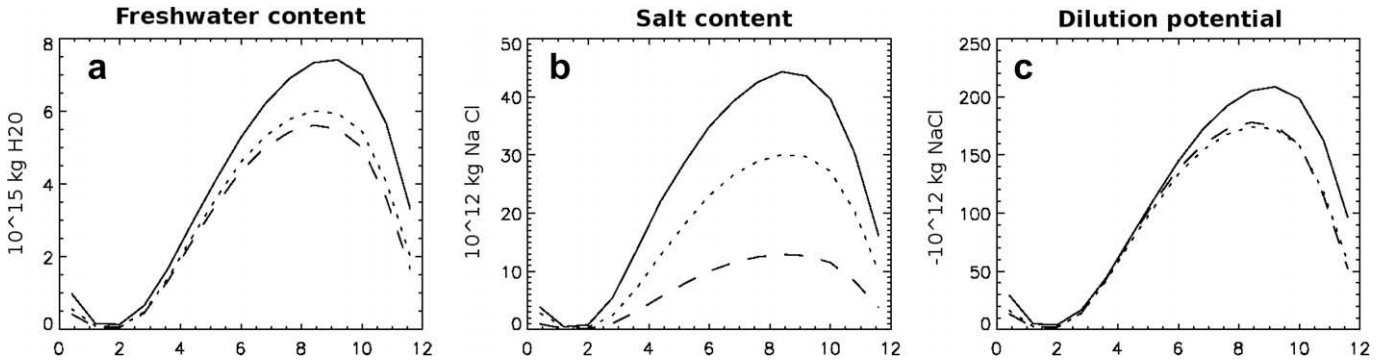

Fig. 11. Mean 1979–2006 seasonal cycle of the total sea ice freshwater content (a), salt content (b) and dilution potential (c) as defined in Section 6.1.2 for the entire SH. Solid lines correspond to SZT-IO, dotted lines to BK5 and dashed lines to PR. Since SZT-I does not conserve salt, it makes no sense to show the associated diagnostics.

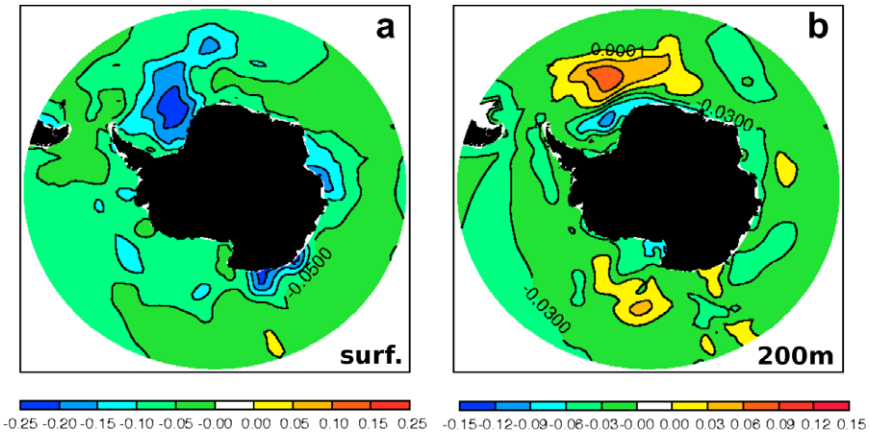

Fig. 12. SZT-IO – BK5 1979–2006 annual differences in oceanic salinity (September) in the SH (a) at the surface and (b) at 200 m depth.

winter F^s in turn maintains fresher surface salinites in SZT-IO compared to the sensitivity runs. In addition, the SST is lower by 0–0.5 °C all over the Southern Ocean.

Vertical mixing and convective activity are also affected, as indicated by the geographical distributions of mixed layer depth in SZT-IO and BK5 (see Fig. 13. First, in the Weddell and Ross Seas, intense vertical mixing on the central regions of the continental shelves disappears in SZT-IO compared to the sensitivity runs: differences in mixed layer depth on the shelf reach as much as 500 m. This is due to the fresher surface waters over the shelves, induced by the reduced ice–ocean salt flux in fall. This suggests that less deep water is formed in SZT-IO, though this is difficult to analyze as our runs are too short for that purpose. Consequently, at 200 m depth, in SZT-IO, salinity is lower than in the sensitivity runs over the shelves (due to smaller F^s) and higher offshore (due to reduced vertical mixing). Second, out of the sea ice zone, at mid-latitudes, in the Atlantic and Pacific Sectors, the mixed layer is shallower by 50–200 m. On the shelves, the simulated mixed layer is clearly improved as no convection should occur there. In the remainder of the ocean, it is difficult to say whether the change in mixed layer depth constitutes an improvement or not, due to the sparsity of data.

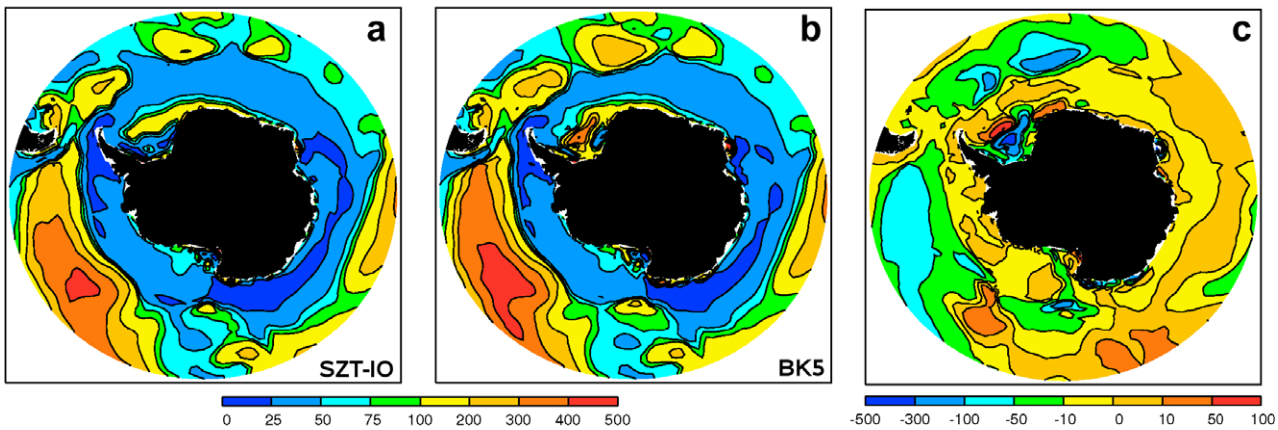

Fig. 13. 1979–2006 winter mixed layer depth (m) in the SH: (a) SZT-IO, (b) BK5 and (c) SZT-IO – BK5 difference.

7. Discussion, conclusions and perspectives

In this paper, we address the question of the importance of large-scale sea ice salinity variations for the sea ice mass balance and the upper ocean. To examine this question, we formulate salinity variations in the framework of the sea ice thickness distribution theory, using a simple parameterization for brine entrapment and drainage. The latter is tested one-dimensionally and then included in a three-dimensional large-scale ice–ocean model, OPA9-LIM3, which is run over 1970–2006. After comparing the simulated 3D salinity field to ice core observations, the role of salinity variations is analyzed by comparing the results of the simulation including the interactive salinity parameterization and several simpler representations of sea ice salinity.

The large-scale features of the simulated ice salinity field can be considered as reliable. First, the brine entrapment and drainage parameterization enables to simulate the seasonal cycle of vertical salinity profile in a 1D landfast sea ice test case rather realistically. Second, the large-scale seasonal cycle of ice salinity simulated by LIM3 compares well with a compilation of ice cores observations at various locations in both hemispheres. The largest model-data discrepancies are found when the observation value comes from a set that does not contain enough measurements to be the exact equivalent of the large-scale model value. Finally, the simulated ice salinity distribution in ice thickness space was compared and found in good agreement with the salinity-thickness relation of Cox and Weeks (1974), both in winter and summer. Scarcity of data renders an accurate model validation difficult. Nevertheless, the general features of the simulated spatio-temporal variations in sea ice salinity seem to be well captured.

The simulated NH and SH salinity fields are quite different. In the NH, in winter, there is an important contrast in ice salinity driven by the relative fractions of FY (thin) and MY (thick) ice, which are characterized by high and low salinities, respectively. In summer, this contrast is wiped out by the percolation of meltwater through the open brine network (flushing), which drastically reduces the sea ice salinity to around 2‰. In the SH, the salinity is higher and the amplitude of the seasonal and spatial variations is lower. This is due to the fact that, in the SH, (1) the contribution of young ice is more important, (2) the frequency of surface melt, and hence of flushing, is much lower, and (3) the contribution of snow ice formation (which traps large amounts of salt) to the global ice mass balance is higher.

In the NH, the findings regarding model sensitivity to salinity variations confirms and extends the results of the 1D study of Vancoppenolle et al. (2006). The role of ice salinity variations in the Arctic mainly consists of a direct impact on the ice thermodynamic processes. Including salinity variations reduces the energy required to melt a unit volume of sea ice. This increases winter bottom and lateral growth rates and produces thicker winter sea ice (from 10 cm to 1 m) in the Arctic Ocean. In summer, using an interactive salinity distribution facilitates the melt of new ice, which has a lower thermal inertia. This leads to higher open water areas, traps more solar radiation, increases the oceanic heat flux and enhances basal melt significantly. Finally, this yields differences in annual mean ice volume up to 11%. In addition, an interactive salinity reduces the ice–ocean salt flux during sea ice growth, which freshens the upper ocean, reduces vertical mixing and slightly weakens deep convection in the North Atlantic. Nevertheless, these changes are not sufficient to induce significant feedbacks on sea ice.

The changes in NH ice thickness due to the inclusion of salinity variations in the model are of the same order of magnitude as changes induced by a 10% change in bare ice albedo (see Fig. 6, panel c). Given the large magnitude of the ice thickness changes, it is crucial to maintain and improve the field observations of sea ice salinity. Note that sea ice models with ITD are much less sensitive to albedo than 1D or single-category ice models. In ice models including ITD, the coupled ice–ocean albedo feedback is governed by the rate of disappearance of thin ice and the amount of open water, while in 1D or single-category models, it is governed by the value of bare ice albedo.

In the SH, the changes in ice thickness are even larger. Because of the weaker vertical oceanic stratification, the influence of a variable salinity on ice–ocean interactions and feedbacks dominates. Using an interactive salinity distribution allows to grow more ice while rejecting less salt into the ocean. This maintains a relatively shallow mixed layer and a low oceanic heat flux, which, in turn, further enhances ice growth. This results in differences in ice volume up to 28%.

We have shown that the sea ice volume and coverage as well as the geographical distribution of ice thickness are sensitive to the model representation of ice salinity. Arctic sea ice is on a track toward a seasonal cover (see, e.g., Serreze et al., 2007). According to models used for the climate projections of the IPCC Fourth Assessment report, this trend should keep on in the 21st century (e.g., Arzel et al., 2006; Zhang and Walsh, 2006). Therefore, as the contribution of FY ice becomes larger and larger, the Arctic sea ice salinity is increasing and will continue to increase in the future. In addition, the subsequent increase in growth of new sea ice will give more winter salt rejection to the ocean, deepen the mixed layer, which could in turn reduce the ice growth rate. Nevertheless, in present sea ice models, salinity is tuned for conditions that prevailed over the 20th century, but which are not adequate for the future sea ice cover. The models used for simulations of future climate should therefore take into account salinity variations. Finally, given the sensitivity of the model to the sea ice salinity, improved physical formulations of sea ice halo-thermodynamics processes (see, e.g., Notz, 2005) are clearly necessary.

Acknowledgements

We gratefully thank Tony Worby, Hajo Eicken, Chris Petrich, Austin Kovacs, Don Perovich, Jean-Louis Tison, Marcel Nicolaus and Christian Haas for providing some of their ice core data. We also thank Cecilia Bitz, Valérie Dulière, Ralph Timmermann, Didier Swingedouw, Austin Kovacs and Ivan Grozny for scientific discussions that helped improving this work, Miguel Angel Morales Maqueda, Chris König, Wouter Lefebvre and two anonymous reviewers for comments that helped to improve this manuscript. M.V. is supported by the Belgian Federal Science Policy Office and FNRS. H.G. is Research Associate with FNRS. This work is done within the framework of the projects BELCANTO (funded by the Belgian Science Federal Policy Office),"A Second-Generation Model of the Ocean System" (funded by Communauté Française de Belgique, ARC 04/09-316) and"Sea-ice biogeochemistry in polar oceans" (funded by FRFC-FNRS).

References

Aagaard, K.A., Carmack, E.C., 1989. The role of sea ice and other fresh water in the Arctic circulation. Journal of Geophysical Research 94, 14485–14498.

Arzel, O., Fichefet, T., Goosse, H., 2006. Sea ice evolution over the 20th and 21st centuries as simulated by current AOGCMs. Ocean Modelling 12, 401–415.

Bates, N.R., 2006. Air-sea CO2 fluxes and the continental shelf pump of carbon in the Chukchi Sea adjacent to the Arctic Ocean. Journal of Geophysical Research 111, C10013. doi:10.1029/2005JC003083.

Baumgartner, F., Reichel, E., 1975. The World Water Balance: Mean Annual Global, Continental and Maritime Precipitation, Evaporation and Runoff. Elsevier, Amsterdam. 179pp.

Berliand, M.E., Strokina, T.G., 1980. Global distribution of the total amount of clouds. Hydrometeorological, Leningrad. 71 pp. (in Russian).

Bitz, C.M., Lipscomb, W.H., 1999. An energy-conserving thermodynamic model of sea ice. Journal of Geophysical Research 104, 15,669–15,677.

Bitz, C.M., Holland, M.M., Weaver, A.J., Eby, M., 2001. Simulating the ice-thickness distribution in a coupled climate model. Journal of Geophysical Research 106, 2441–2463.

Bouillon, S., Morales Maqueda, M.A., Fichefet, T., Legat, V., 2009. An elastic-viscous-plastic sea ice model formulated on Arakawa B and C grids. Ocean Modelling, submitted for publication.

Cavalieri, D.J., Parkinson, C.L., Vinnikov, K.Y., 2003. 30-year satellite record reveals contrasting Arctic and Antarctic sea ice variability. Geophysical Research Letters 30 (18), 1970. doi:10.1029/2003GL018031.

Comiso, J.C., 2006. Abrupt decline in the Arctic winter sea ice cover. Geophysical Research Letters 33, L18504. doi:10.1029/2006GL027341.

Comiso, J.C., 2007. Bootstrap sea ice concentrations from NIMBUS-7 SMMR and DMSP SSM/I, 1979–2006. Boulder, Colorado USA: National Snow and Ice Data Center. Digital Media.

Cottier, F., Eicken, H., Wadhams, 1999. Linkages between salinity and brine channel distribution in young sea ice. Journal of Geophysical Research 104, 15,859–15,871.

Cox, G.F.N., Weeks, W.F., 1974. Salinity variations in sea ice. Journal of Glaciology 13, 109–120.

Cox, G.F.N., Weeks, W.F., 1975. Brine drainage and initial salt entrapment in sodium chloride ice. CRREL Report 345, 85. US Army Cold Reg. Res. and Eng. Lab., Hanover, NH.

Cox, G.F.N., Weeks, W.F., 1988. Numerical simulations of the profile properties of undeformed first-year sea ice during growth season. Journal of Geophysical Research 93, 12,449–12,460.

de Boyer Montégut, C., Madec, G., Fischer, A.S., Lazar, A., Iudicone, D., 2004. Mixed layer depth over the global ocean: an examination of profile data and a profile-based climatology. Journal of Geophysical Research 109, C12003. doi:10.1029/2004JC002378.

Delille, B., 2006. Inorganic carbon dynamics and air–ice–sea CO_2 fluxes in the open and coastal waters of the Southern Ocean. Ph.D. Thesis. Université de Liège, Liège, Belgium.

Ebert, E.E., Curry, J.A., 1993. An intermediate one-dimensional thermodynamic sea ice model for investigating ice–atmosphere interactions. Journal of Geophysical Research 98, 10085–10109.

Eicken, H., 1992. Salinity profiles of Antarctic sea ice: field data and model results. Journal of Geophysical Research 97, 15,545–15,557.

Eicken, H., 1998. Factors determining microstructure, salinity and stable isotope composition of Antarctic sea ice: deriving modes and rates of ice growth in the Weddell Sea. In: Jeffries, M.O. (Ed.), Antarctic Sea Ice: Physical Processes, Interactions and Variability, Antarctic Research Series, vol. 74. AGU, Washington, DC, pp. 89–122.

Eicken, H., Proshutinsky, A., 2005. Thickness, salinity and stable isotope composition of sea ice samples from the Laptev Sea, 1999. National Snow and Ice Data Center, Boulder, CO, USA. digital media.

Eicken, H., Lange, M.A., Dieckmann, G.S., 1991. Spatial variability of sea ice properties in the northwestern Weddell Sea. Journal of Geophysical Research 96, 10,603–10,615.

Eicken, H., Gow, A.J., Salmela, O., 1995. Thickness, structure, and properties of level summer multiyear ice in the Eurasian sector of the Arctic Ocean. Journal of Geophysical Research 100 (C11), 22,697–22,710.

Fichefet, T., Morales Maqueda, M.A., 1997. Sensitivity of a global sea ice model to the treatment of ice thermodynamics and dynamics. Journal of Geophysical Research 102, 12,609–12,646.

Frankenstein, G., Garner, R., 1967. Equations for determining the brine volume of sea ice from −0.5°C to −22.9°C. Journal of Glaciology 6, 943–944.

Gerland, S., Winther, J.-G., Ørbaek, J.B., Ivanov, B., 1999. Physical properties, spectral reflectance and thickness development of first year fast-ice in Kongsfjorden, Svalbard. Polar Research 18 (2), 275–282.

Goosse, H., Fichefet, T., 1999. Importance of ice–ocean interactions for the global ocean circulation: a model study. Journal of Geophysical Research 104, 23337–23355.

Gow, A.J., Tucker III, W.B., 1990. Sea ice in the polar regions. In: Smith, W.O. (Ed.), Polar Oceanography, Polar Oceanography, Part A, Physical Science. Academic Press, San Diego, USA, pp. 47–122.

Gow, A.J., Ackley, S.F., Buck, K.R., Golden, K.M., 1987. Physical and structural characteristics of Weddell Sea pack ice. CRREL Report, 87-14.

Gow, A.J., Ackley, S.F., Govoni, J.W., Weeks, W.F., 1998. Physical and structural properties of land-fast sea ice in McMurdo Sound, Antarctica. In: Jeffries, M.O. (Ed.), Antarctic Sea Ice: Physical Processes, Interactions and Variability, Antarctic Research Series, vol. 74. American Geophysical Union, Washington, DC, pp. 355–374.

Granskog, M.A., Leppäranta, M., Kawamura, T., Ehn, J., Shirasawa, K., 2004. Seasonal development of the properties and composition of landfast sea ice in the Gulf of Finland, the Baltic Sea. Journal of Geophysical Research 109, C02020. doi:10.1029/2003JC001874.

Grenfell, T.C., Perovich, D.K., Eicken, H., Light, B., Harbeck, J., George, T.G., Mahoney, A., 2006. Energy and mass balance observations of the land–ice–ocean–atmosphere system near Barrow, Alaska November 1999–July 2002. Annals of Glaciology 44, 193–199.

Hellmer, H.H., Haas, C., Dieckmann, G.S., Schröder, M., 2006. Sea ice feedbacks observed in western Weddell Sea. EOS 87 (18), 173–179.

Holland, M.M., Bitz, C.M., Hunke, E.C., Lipscomb, W.H., Schramm, J., 2006a. Influence of the sea ice thickness distribution on polar climate in CCSM3. Journal of Climate 19, 2398–2414.

Holland, M.M., Bitz, C.M., Tremblay, B., 2006b. Future abrupt transitions in the summer Arctic sea ice. Geophysical Research Letters 33, L23503. doi:10.1029/2006GL028024.

Hunke, E.C., Lipscomb, W.H., 2004. CICE: The Los Alamos Sea Ice Model, documentation and software user's manual, version 3. LACC-98-16, Los Alamos National Laboratory, Los Alamos, New Mexico.

Jeffries, M., Porter, M., 1995. Sea-ice development in the Ross, Amundsen, and Bellingshausen Seas revealed by analysis of ice cores in late winter 1993 and 1994. Antarctic Journal 30, 16–18.

Jeffries, M.O., Worby, A.P., Morris, K., Weeks, W.F., 1997. Seasonal variations in the properties and structural composition of sea ice and snow cover in the Bellingshausen and Amundsen Seas, Antarctica. Journal of Glaciology 43, 138–151.

Kalnay, E., Kanamitsu, M., Kistler, R., Collins, W., Deaven, D., Gandin, L., Iredell, M., Saha, S., White, G., Woollen, J., Zhu, Y., Leetmaa, A., Reynolds, B., Chelliah, M., Ebisuzaki, W., Higgins, W., Janowiak, J., Mo, K., Ropelewski, C., Wang, J., Jenne, R., Joseph, D., 1996. The NCEP/NCAR 40-year reanalysis project. Bulletin of the American Meteorological Society 77, 437–471.

Kovacs, A., 1996. Sea ice, part I, Bulk salinity versus ice floe thickness. CRREL Report 96–7, 16. US Army Cold Reg. Res. and Eng. Lab., Hanover, NH.

Large, W.G., Yeager, S.G., 2004. Diurnal to decadal global forcing for ocean and sea ice models: the data sets and climatologies. NCAR Technical Report, TN-460+STR, 105 pp.

Lipscomb, W.H., 2001. Remapping the thickness distribution in sea ice models. Journal of Geophysical Research 106 (C7), 13,989–14,000.

Madec, G., 2008. NEMO reference manual, ocean dynamics component: NEMO-OPA. Preliminary version. Note du Pole de modélisation, Institut Pierre-Simon Laplace (IPSL), France, No. 27 ISSN No. 1288-1619.

Malmgren, F., 1927. On the properties of sea ice. In: Sverdrup, H.U. (Ed.), The Norwegian North Polar Expedition with the 'Maud' 1918–1925, vol. 1a(5). John Griegds Boktr., Bergen, Norway, pp. 1–67.

Marshall, J., Schott, F., 1999. Open-ocean convection: observations, theory and models. Review of Geophysics 37 (1), 1–64.

Maykut, G.A., 1986. The surface heat and mass balance. In: Untersteiner, N. (Ed.), The Geophysics of Sea Ice, NATO ASI Series B: Physics, vol. 146. Plenum Press, New York, pp. 395–464.

Maykut, G.A., Untersteiner, N., 1971. Some results from a time-dependent thermodynamic model of sea ice. Journal of Geophysical Research 76, 1550–1575.

Nakawo, M., Sinha, N.K., 1981. Growth rate and salinity profile of first-year sea ice in the high Arctic. Journal of Glaciology 27, 315–331.

Notz, D., 2005. Thermodynamic and fluid-dynamical processes in sea ice. Ph.D. Thesis. University of Cambridge, UK.

Perovich, D.K., Elder, B.C., Claffey, K.J., Stammerjohn, S., Smith, R., Ackley, S.F., Krouse, H.R., Gow, A.J., 2004. Winter sea-ice properties in Marguerite Bay, Antarctica. Deep-Sea Research II 51, 2023–2039.

Prather, M., 1986. Numerical advection by conservation of second-order moments. Journal of Geophysical Research 91, 6671–6681.

Pringle, D.J., Eicken, H., Trodahl, H.J., Backstrom, L.G.E., 2007. Thermal conductivity of landfast Antarctic and Arctic sea ice. Journal of Geophysical Research 112, C04017. doi:10.1029/2006JC003641.

Rothrock, D.A., Percival, D.B., Wensnahan, M., 2008. The decline in arctic sea-ice thickness: separating the spatial, annual, and interannual variability in a quarter century of submarine data. Journal of Geophysical Research 113, C05003. doi:10.1029/2007JC004252.

Schramm, J.L., Holland, M.M., Curry, J.A., Ebert, E.E., 1997. Modeling the thermodynamics of a sea ice thickness distribution. 1. Sensitivity to ice thickness resolution. Journal of Geophysical Research 102 (C10), 23,079–23,091.

Schwarzacher, W., 1959. Pack-ice studies in the Arctic Ocean. Journal of Geophysical Research 64, 2357–2367.

Serreze, M.C., Holland, M.M., Stroeve, J., 2007. Perspectives on the Arctic's shrinking sea-ice cover. Science 315, 1533–1536. doi:10.1126/science.1139426.

Steele, M., Morley, R., Ermold, W., 2001. PHC: a global ocean hydrography with a high quality Arctic Ocean. Journal of Climate 14, 2079–2087.

Thomas, D.N., Dieckmann, G.S., 2002. Antarctic sea ice – a habitat for extremophiles. Science 295, 641–644.

Thorndike, A.S., Rothrock, D.A., Maykut, G.A., Colony, R., 1975. The thickness distribution of sea ice. Journal of Geophysical Research 80, 4501–4513.

Timmermann, R., Goosse, H., Madec, G., Fichefet, T., Ethé, C., Dulière, V., 2005. On the representation of high-latitude processes in the ORCALIM global coupled sea ice–ocean model. Ocean Modelling 8, 175–201.

Tison, J.-L., Worby, T., Delille, B., Brabant, F., Papadimitriou, S., Thomas, D.N., de Jong, J., Lannuzel, D., Haas, C., 2008. Thermodynamic evolution of decaying summer first-year sea ice at ISPOL (Western Weddell Sea, Antarctica). Deep Sea Research II 55 (8), 975–987.

Trenberth, K.E., Olson, J.G., Large, W.G., 1989. A global ocean wind stress climatology based on the ECMWF analyses. National Center for Atmospheric Research, Boulder, Colorado, NCAR/TN-338+STR, 93 pp.

Tucker, W.B., Gow, A.J., Richter, J.A., 1984. On small-scale horizontal variations of salinity in first-year sea ice. Journal of Geophysical Research 89 (C10), 6505–6514.

Tucker III, W.B., Gow, A.J., Weeks, W.F., 1987. Physical properties of summer sea ice in the Fram Strait. Journal of Geophysical Research 92, 6787–6803.

Tucker III, W.B., Gow, A.J., Meese, D.A., Bosworth, H.W., Reimnitz, E., 1999. Physical characteristics of summer sea ice across the Arctic Ocean. Journal of Geophysical Research 104 (C1), 1489–1504.

Vancoppenolle, M., Fichefet, T., Bitz, C.M., 2005. On the sensitivity of undeformed Arctic sea ice to its vertical salinity profile. Geophysical Research Letters 32, L16502. doi:10.1029/2005GL023427.

Vancoppenolle, M., Fichefet, T., Bitz, C.M., 2006. Modeling the salinity profile of undeformed Arctic sea ice. Geophysical Research Letters 33, L21501. doi:10.1029/2006GL028342.

Vancoppenolle, M., Bitz, C.M., Fichefet, T., 2007. Summer land fast sea ice desalination at Point Barrow, Alaska: model and observations. Journal of Geophysical Research 112, C04022. doi:10.1029/2006JC003493.

Vancoppenolle, M., Fichefet, T., Goosse, H., Bouillon, S., Morales Maqueda, M.A., 2009. Simulating the mass balance and salinity of Arctic and Antarctic sea ice. 1. Model description and validation. Ocean Modelling 27 (1–2), 33–53.

Weeks, W.F., Lee, O.S., 1958. Observations on the physical properties of sea ice at Hopedale, Labrador. Arctic 11 (3), 134–155.

Weeks, W.F., Lee, O.S., 1962. The salinity distribution in young sea ice. Arctic 15 (2), 92–108.

Widell, K., Fer, I., Haugan, P.M., 2006. Salt release from warming sea ice. Geophysical Research Letters 33, L12501. doi:10.1029/2006GL026262.

Worby, A.P., Massom, R.A., Allison, I., Lytle, V., Heil, P., 1998. East Antarctic sea ice: a review of its structure, properties and drift. In: Jeffries, M.O. (Ed.), Antarctic Sea Ice: Physical Processes, Interactions and Variability, Antarctic Research Series, vol. 74. AGU, Washington, DC, pp. 89–122.

Worby, A.P., Geiger, C.A., Paget, M.J., Van Woert, M.L., Ackley, S.F., DeLiberty, T.L., 2008. The thickness distribution of Antarctic sea ice. Journal of Geophysical Research 113, C05S92. doi:10.1029/2007JC004254.

Zhang, J., Rothrock, D.A., 2001. A thickness and enthalpy distribution sea-ice model. Journal of Physical Oceanography 31, 2986–3001.

Zhang, X., Walsh, J.E., 2006. Toward a seasonally ice-covered Arctic Ocean: scenarios from the IPCC AR4 Model simulations. Journal of Climate 19, 1730–1747.